

Electronic Spectra of Trigonal and Disordered Phases of Tellurium and Selenium. II. Experiment

L. D. Laude

Surface Physics Division, European Space Research Organisation, Noordwijk, Holland

B. Kramer

Institut für Physik der Universität Dortmund, Germany

K. Maschke

Abteilung für Physik der Universität Marburg, Germany

(Received 20 February 1973)

The electronic structures of trigonal tellurium and trigonal selenium have been investigated by photoemission, using conventional energy-distribution curves (EDC's) and their second derivatives which reveal significant fine structure, embedded, but hardly observable, in EDC's. The two p valence bands (p_1 and p_2) and the second conduction band (SCB) are explored for both materials except for p_1 in the case of Se. In particular, the bottom of the SCB is positioned 4.6 and 6.1 eV above the upper edge of p_2 in Te and Se, respectively. The spectral structure is interpreted in terms of partial contributions to the total density of states (DOS) of restricted regions of the Brillouin zone, namely, about the Δ axis and point H , as obtained theoretically in Paper I of this work. A similar study is carried out on disordered films of Te and Se, deposited in ultrahigh vacuum onto a flame-polished silica substrate. A comparison between the photoemission spectra obtained from these films and those obtained from trigonal Te and Se reveal a sharp attenuation of the conduction-band-DOS structure in agreement with the theoretical results, Paper I. The valence-band total DOS in these films exhibit more subtle disorder effects, characterized by (i) the loss of the contribution of point H and (ii) the preservation of the Δ contribution. In addition, it is shown that, depending on the thermal treatment of the films, two sets of disordered configurations may be obtained in Te: one [α -Te(1)] which can effectively be approximated by disordering the trigonal Te lattice, and the other [α -Te(2)] which represents a further departure from this lattice and could, therefore, be approached via deformation of a different (possibly simple cubic) lattice. Because of the relatively good fit achieved in the experimental electronic structure of the disordered Se films using the trigonal approach, these films do not seem to contain a majority of Se_8 rings but might rather consist of a mixture of small weakly distorted Se chains, possibly amalgamated with a small proportion of rings.

I. INTRODUCTION

In the previous paper (Paper I of this work),¹ calculations of the electronic structure of both tellurium and selenium have been presented. They were based on a pseudopotential calculation performed by Sandrock² for trigonal Se and by Maschke³ for trigonal Te. The results have shown well-characterized disorder effects on the density of states of these two materials. In this paper, photoemission data are presented which (i) support the band-structure calculations of the crystalline phases of these two elements, in particular by exploring regions of their electronic structure that could not be investigated accurately using optical-absorption measurements, and (ii) illustrate the anticipated disorder effects present in their amorphous configurations.

Though the photoemissive properties of Te and Se are of a current practical interest, previous uv-photoemission data were only scarce for these materials⁴⁻¹⁰ and dealt in most cases with photoelectric-yield measurements which cannot bring direct and precise information on the density of

states. In the present work, emphasis is put on the fine structure existing in photoelectron energy-distribution curves (EDC's) obtained from ultrahigh-vacuum cleaved (10 $\bar{1}$ 0) Te and Se in the photon energy ranges 5-9 eV (Te) and 6-11 eV (Se). This fine structure is known to be strongly enhanced by higher-derivative techniques,^{11,12} and these were used here systematically in parallel with conventional EDC analysis. The interpretation of the relevant spectral features is obtained by a comparison with the partial contributions to the total density of states, originating from restricted regions of the Brillouin zone, as calculated in Ref. 1. Preliminary results of this study were already published.^{12,13}

Apart from new information collected on the band structures of trigonal Te and Se, emphasis is placed on a comparison between the electronic properties of the crystalline and disordered phases of these elements, as seen from the photoemission point of view, in the light of the complex-band-structure calculations presented in Ref. 1. In particular, disorder is seen to affect not only the conduction-band but also the valence-band density of states of these elements, depending on the thermal

treatment of films prepared and maintained in ultra-high vacuum ($< 2 \times 10^{-10}$ torr) onto flame-polished silica substrates. Finally, a comparison between the disordered and trigonal forms of Te and Se allows some conclusions to be drawn concerning the configurational properties of these materials in their disordered phases.

Sharp polarization effects were observed in both crystalline materials, as expected from their strong anisotropy. The description of these effects, together with their interpretation, will be subsequently presented in a separate publication.¹⁴

II. PHOTOEMISSION AND DENSITY OF STATES: CASE OF Se AND Te

The information resulting from the usual optical-absorption measurements¹⁵⁻²⁴ is restricted by the fact that one measures only the energy differences between initial and final states. In the photoemission process, the number of emitted electrons that are first directly excited to a final-state energy level \mathcal{E} , can be approximated by^{25,26}

$$N(\mathcal{E}, \omega) = \sum_{v,c} \int_{\mathbf{k}} |M_{cv}(\mathbf{k})|^2 \delta(\mathcal{E} - E_{v,\mathbf{k}} - \hbar\omega) \times \delta(\mathcal{E} - E_{c,\mathbf{k}}) \mathcal{P}(\mathcal{E}, \mathbf{k}) d^3\mathbf{k}, \quad (1)$$

where $|M_{cv}(\mathbf{k})|^2$ is the probability for an optical transition from the valence-band energy level $E_{v,\mathbf{k}}$ to the conduction-band energy level $E_{c,\mathbf{k}}$ to occur. $\mathcal{P}(\mathcal{E}, \mathbf{k})$ is the escape probability. For simplicity, we assume that $\mathcal{P}(\mathcal{E}, \mathbf{k})$ is independent of \mathbf{k} and

$$\mathcal{P}(\mathcal{E}, \mathbf{k}) = P(\mathcal{E}) = 1 \quad \text{for } \mathcal{E} \geq E_0 \\ = 0 \quad \text{for } \mathcal{E} < E_0, \quad (2)$$

E_0 is the vacuum-level energy at the surface.

Evaluation of the volume integral on the right-hand side of Eq. (1) yields the energy-distribution function as a line integral in \mathbf{k} space, the lines being given by the conditions

$$E_{c,\mathbf{k}} - E_{v,\mathbf{k}} = \hbar\omega, \quad E_{c,\mathbf{k}} = \mathcal{E}. \quad (3)$$

The energy-distribution curve (EDC), $N(\mathcal{E}, \omega)$, exhibits van Hove singularities if the expression $[\nabla_{\mathbf{k}}[E_{c,\mathbf{k}} - E_{v,\mathbf{k}}] \times \nabla_{\mathbf{k}}E_{c,\mathbf{k}}]_{\mathbf{k}=\mathbf{k}_0}$ vanishes, \mathbf{k}_0 fulfilling the conditions set by Eq. (3). The form of the singularities is determined by the topology of the respective critical lines.²⁶ The intensity of the singularities is mainly determined by the optical-transition matrix element multiplied by the escape probability. For some special cases, one can correlate qualitative features of the EDC's to the density of states by inspection of Eq. (1). If one takes, for instance, the conduction band to be nearly independent of \mathbf{k} , i. e., the conduction-band density of states (DOS) is characterized by one single peak ($E_{c,\mathbf{k}} = E_c$), then, from Eq. (1) and taking the oscil-

lator strength to be constant in \mathbf{k} space

$$N(\mathcal{E}, \omega) \sim \delta(\mathcal{E} - E_c) n_v(\mathcal{E} - \hbar\omega), \quad (4)$$

where $n_v(\mathcal{E} - \hbar\omega)$ is the valence-band DOS. This will correspond to a sharp peak in the EDC, remaining stable in final-state energy $\mathcal{E} = E_c$. If there is one peak in the valence-band DOS ($E_{v,\mathbf{k}} = E_v$), one obtains

$$N(\mathcal{E}, \omega) \sim \delta(\mathcal{E} - E_v) n_c(\mathcal{E}), \quad (5)$$

where $n_c(\mathcal{E})$ is the conduction-band DOS. This corresponds to a peak in the EDC that now varies with photon energy according to

$$\mathcal{E} = E_v + \hbar\omega. \quad (6)$$

So, by tracing the behavior of a given peak in the EDC with photon energy, one can assign this peak to a valence- or a conduction-band DOS feature. The intermediate cases between Eqs. (4) and (5) will appear in an $(\mathcal{E}, \hbar\omega)$ energy diagram as a bending and branching of the lines,²⁸ which describe the behavior of either conduction- or valence-band peaks on such a diagram. The same arguments yielding Eqs. (4) and (5) hold also if the \mathbf{k} dependence of the energy bands is negligible only in some regions of the Brillouin zone. Due to the fact that the bands are relatively flat in Se and Te (Figs. 5 and 6 of Ref. 1), these conditions may be considered to be sufficiently well satisfied for these two materials.

The case of a disordered solid may also be described by Eq. (1) if the real energy bands $E_{v,\mathbf{k}}$ and $E_{c,\mathbf{k}}$ are replaced by complex energy bands: $\epsilon_{v,\mathbf{k}} = E_{v,\mathbf{k}} + i\Gamma_{v,\mathbf{k}}$ and $\epsilon_{c,\mathbf{k}} = E_{c,\mathbf{k}} + i\Gamma_{c,\mathbf{k}}$, in analogy with Eq. (21) of Ref. 1, for the density of states. As a consequence, one may use similar arguments, as in the crystalline case, to interpret the $(\mathcal{E}, \hbar\omega)$ behavior of the EDC features in the disordered phase.

The application of such considerations are, of course, restricted to transitions towards conduction-band states lying above the surface-potential barrier. Because of the high values of the photoelectric threshold E_T , measured to be 4.65 ± 0.05 eV in the case of trigonal Te and 6.1 ± 0.2 eV in the case of trigonal Se, no information on the p_3 band could be obtained from the photoemission data.²⁷ The s valence band starts 9 and 7 eV below valence-band edge for Se and Te, respectively.²⁸ Transitions between the s valence band and the second conduction band (SCB) could therefore start contributing to the photoemission spectra at photon energies higher than ~ 15 eV for Se and 11.5 eV for Te. These energies were not reached in this work and no information on the s band could be obtained. In addition, it is expected that at these energies the spectra could be perturbed significantly by inelastic electron-electron scattering, as shown by

Nielsen¹⁰ in the case of amorphous selenium and, to a lesser extent, in this work in the case of trigonal tellurium.

The overall agreement between experiment and theory was found to be satisfactory for the p_1 and p_2 bands in Te and Se, and for SCB in Se. The theoretical fit to this latter band in Te was obtained by shifting the calculated SCB by 1.2 eV to lower energy.

III. EXPERIMENTAL

The photoemission data were obtained from high-purity vacuum-cleaved single crystals and from disordered films prepared in ultra-high vacuum. The Te crystals were grown using the Czolchzalski method. They were p type and their resistivity was measured to be constant at 0.3 Ω cm at 300 °K all along the crystals. The room-temperature carrier density was estimated to be about 5×10^{15} cm⁻³.²⁹ A Bridgman technique was used to prepare the thallium-doped Se crystals,³⁰ which were also p type. Their resistivity was that typical of such Se single crystals, i. e., $\sim 10^6$ Ω cm.

Surface contamination is known to perturb drastically the behavior of the photoexcited electrons, which reach the surface and then scatter within the contaminant before being emitted in vacuum. Therefore, it appeared essential to cleave the crystals used in this experiment in ultra-high vacuum, the actual working pressure being always maintained in the 10^{-11} -torr range. Residual-gas analysis has shown the presence of traces of H₂ but none of oxygen.

Figure 1(a) gives a schematic view of the experimental setup. Details of the cleaver were presented elsewhere.³¹ The Te samples were x-ray-oriented parallelepipeds of dimensions $4 \times 2 \times 15$ mm, having (10 $\bar{1}0$) end faces (cleaving plane) to $\pm 1^\circ$ accuracy (c axis parallel to the longer edges of the rectangular cross section). Selenium cleaves also along (10 $\bar{1}0$) faces. However, its handling is made difficult owing to its softness. The samples used in this work were single-crystal cylindrical bars, diameter 7 mm approximately, grown perpendicular to c axis. They were mounted directly on their holder in such a way that the cleaving could occur along (10 $\bar{1}0$) faces. In order to minimize any possible rearrangement of atoms in the Te and Se films, these were deposited onto plane, circular, flame-polished, fused-quartz substrates (diameter, 4 mm), cemented at the extremity of a copper holder and maintained at room temperature in the case of Se and 100 °K for Te. The films were electrically connected to the holder via a gold-film contact, previously vacuum-plated on one side of the substrate. Ordering induced by the substrate into the films was illustrated by depositing a Te film onto a polycrystalline gold film previously condensed on

the fused-quartz substrate. Before deposition of the material studied, the substrate was pushed forward linearly and positioned within a 5-mm-diam. window bored into the analyzer. The evaporation source was the same material that was used for the crystalline study. The source-to-substrate distance was 15 cm and the evaporation beam was collimated to obtain a normal incidence deposition at approximately 20-Å/sec rate. Possible perturbation of the analyzer work function by deposition of the evaporated material onto the internal surface of the analyzer was avoided by positioning an 8-mm-diam. copper disk behind the substrate as shown in Fig. 1(a). The Se films were 300–500 Å thick and exhibited the well-known red transparency. The Te films were somewhat thicker (in the range 500–1000 Å). Diffuse halo x-ray diffraction patterns were obtained from the Se films and from the as-deposited Te films prepared at 100 °K and slowly annealed to 300 °K [α -Te(1)]. No diffraction study was carried out on the Te films, after annealing to temperatures higher than 300 °K.

By classical x-ray diffraction standards, the Se and α -Te(1) films prepared as mentioned above should be considered as "amorphous." However, it is stressed that this diffraction technique has a finite resolution limit of some 15–20 Å. Any perfect crystalline ordering present in a film but confined below that limit could not be detected. It is, however, clear that, were the relevant film classified "amorphous," such an ordering should be sufficient, in principle, to rebuild a band structure similar to the crystal one.

On the other hand, Te films, which were deposited at low temperatures but in a much lower vacuum and on a different substrate,²¹ have shown transport properties comparable to the crystalline ones when their temperature was raised above 270 °K. Using that criterium, Te films were then arbitrarily defined as being (i) "amorphous" when maintained at temperatures below that limit and (ii) as "polycrystalline" above. Keeping in mind that such a limit may vary widely depending on film preparation, it is pointed out in addition that a conductivity study does not allow one to investigate the electronic structure of a crystal and *a fortiori* of its disordered configurations, typically in the case of such anisotropic materials like Te and Se.

From these remarks, it appears then superficial, if not simplistic, to try to classify the films between amorphous, polycrystalline, or else, disordered polycrystalline, films, which all represent various degrees of disorder. For this reason, all films prepared in this work will be quoted as disordered.

The sample holder is mounted at the extremity of a copper arm fixed to an insulated copper feedthrough. The exact positioning of the sam-

ple is provided by a manipulator, allowing a 3.8-mm linear-motion drive and tilting of the sample about the feedthrough axis. While the cleaved Te faces were observed to be almost completely free of scratches, the Se ones exhibited bright areas together with a few fibers standing parallel to the c axis. After either cleaving the crystals or after preparation of the film, the sample is moved to-

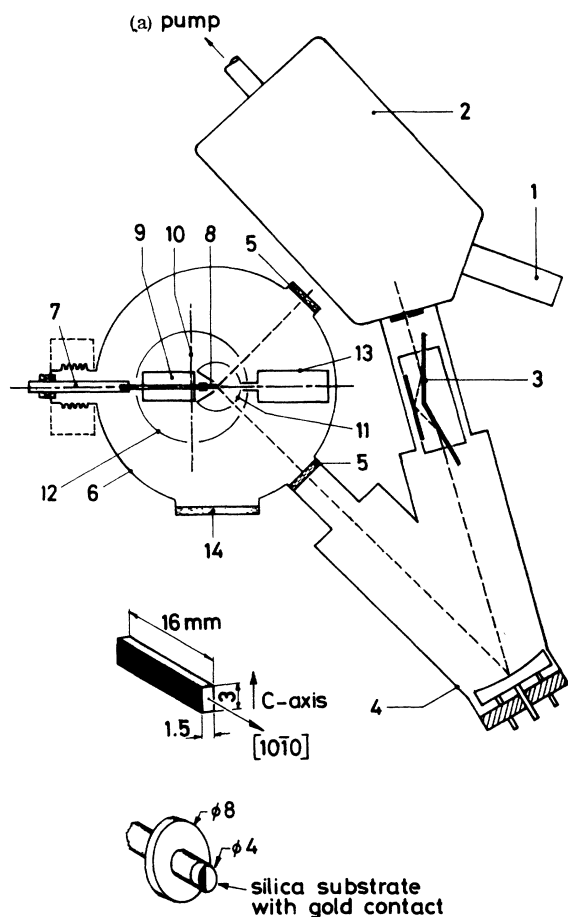
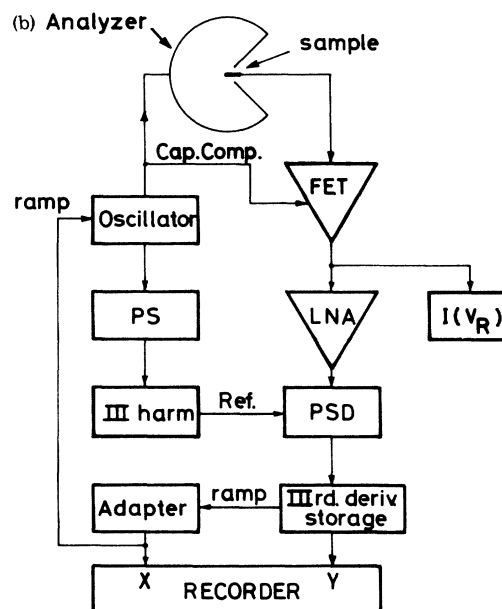


FIG. 1. (a) Experimental setup showing: 1—light source; 2—Mac Pherson 218 uv monochromator; 3—rotating polarizer; 4—(LiF coated) Al spherical mirror, mounted at 17° incidence in an evacuated tube; 5—LiF windows; 6—ultra-high-vacuum chamber; 7—insulated sample holder, mounted on a manipulator model UMD-1 from Vacuum Generators, England; 8—sample clamped at the end of holder; 9—nonmagnetic, stainless-steel crystal cleaver (Ref. 31); 10—cleaving plane; 11—gold-coated spherical electron-energy analyzer; 12—Mu-metal magnetic shielding can; 13—evaporator; 14—viewing port. The geometry and dimension (mm) of the trigonal Te bars used are shown, as well as details of the mounting of the silica substrate used for preparing the Te and Se films. (b) Block diagram of the electronics system used for measuring the energy-distribution curves and their second derivatives. The ramp sweep dc voltage on the spherical analyzer is provided by the screen sweep of a Hewlett-Packard 5480A memory display, adjusted via an adapter to fit the extent of the actual spectrum. Part of this sweep voltage is used for capacitance compensation of the field-effect-transistor (FET) differential amplifier, where the photocurrent is first preamplified. This current then enters a Brookdeal 450 low-noise amplifier (LNA), and further a Brookdeal 411 phase-sensitive detector (PSD). The reference signal to this PSD can either be (i) a 40 hz ac voltage provided by a Hewlett-Packard 204D oscillator via a Brookdeal 421 phase shifter (PS) (to allow measurement of the first derivative of the photocurrent—EDC—at the PSD output), or (ii) the third harmonic (120 Hz) of this ac signal, via the overloaded phase shifter and a Hewlett-Packard 3410A ac μ V meter tuned on that frequency (to measure the third derivative of the photocurrent, after filtering out all other harmonics). The first or third derivative of the photocurrent can then either be directly recorded as a function of the ramp-sweep voltage on an x-y recorder or (for current $\leq 10^{-12}$ A) stored into the memory and displayed at convenience after the noise has been cleared out of the derived signal by the averaging process in the memory.

wards the center of a spherical electron-energy analyzer. The geometry of this analyzer has been corrected to allow the electric field dispersion to be perfectly spherical in the hemisphere in front of the sample impact face. In addition, the cleaver-analyzer assembly is contained in a magnetic shielding can to reduce the magnetic field to less than 0.1 G in the analyzer. The average dimension (a) of the latter being small with regard to the inner diameter (b) of the analyzer ($a/b < \frac{1}{10}$), the energy resolution of the analyzer $\Delta E_k/E_k$ (E_k being the kinetic energy of the emitted electron) can be reasonably estimated³² to be of the order of $\leq 1\%$.

The excitation beam is provided by a hydrogen or mercury lamp mounted at the input slit of a McPherson 218 uv monochromator. Calibration of the source was carried out using a calibrated thermo-



pile, with interpolation by a sodium salicylate target and a photomultiplier. The beam is focussed on the cleaved face under a 45° angle of incidence through a LiF window using a spherical mirror, sample-to-mirror distance being equal to the focal length of the mirror. Before and after reflection onto the cleaved face, the beam passes through ports bored into the analyzer (10-mm diam.) and the shielding can (15-mm diam.). The analyzer ports introduce local disturbance of the electric field inside the analyzer. However, their dimension is small enough to maintain the over-all spherical symmetry of this field³¹ while keeping the largest possible acceptance angle at the sample. The dimension and shape of the slit image (< 1 -mm cross section) are such that the beam can be focussed within the target-face width by adjusting both mirror and sample in concordance. A rotating polarizer, consisting of three gold-coated plane mirrors, could be mounted on axis to provide polarized light.

In that configuration, a sweep-retarding voltage V_R is applied onto the gold-coated interior face of the spherical analyzer and the photocurrent is measured negatively on the sample itself via the insulated feedthrough (leakage resistance of the order of $10^{15-16} \Omega$). A small ac voltage v is superimposed on V_R , which allows EDC's to be monitored by measuring the first-derivative of the photocurrent. The resolution of the entire arrangement described here was evaluated taking into account the scattering of light within the monochromator slits (130 meV for a 1-mm slit opening at $h\nu = 7.72$ eV), the band broadening with temperature ($\approx kT$ or 25 meV at 300 °K) and the analyzer resolution itself as a function of the electron kinetic energy E_k measured above vacuum level. As an example, the energy resolution is found to be 170 meV for $E_k = 1.5$ eV, slit opening $s = 1$ mm and $h\nu = 7.7$ eV. This resolution compares well with those obtained for other analyzer geometries.³³

The usual EDC's measured on Te and Se, both in their crystalline and disordered phases, indicated structure that suggested that the improved visibility afforded by higher-derivative spectroscopy might be used to advantage in this case.^{4,5} Details of the electronic higher-derivation setup are shown in Fig. 1(b).

Higher-derivative spectra were compared with the conventional EDC's measured at the same photon energies. An example of such curves is shown in Fig. 2(a). They were obtained from trigonal Te at $h\nu = 5.49$ eV. At that energy, the EDC (measured with $v = 0.3$ -V peak-to-peak (p.p.) and $s = 1$ mm) is an almost perfect symmetric curve about its maximum, with a width at mid-height of 0.60 eV. These characteristics are observed to be unaffected by decreasing v to 0.15 V p.p. Reducing

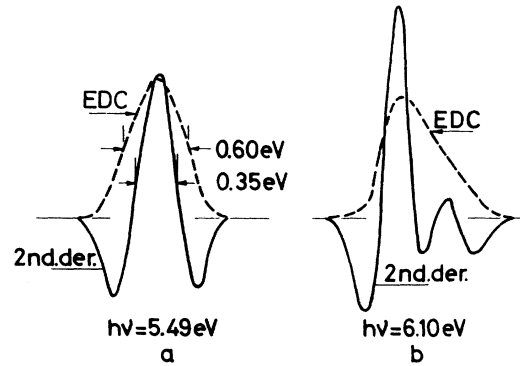


FIG. 2. EDC's and their second derivatives obtained at (a) $h\nu = 5.49$ eV and (b) $h\nu = 6.10$ eV, from a vacuum cleaved (10I0) Te face.

the slit openings does cause a sharpening of the low- and high-energy onsets of the curve, but does not alter the over-all profile of the EDC.³⁴ The second derivative of the EDC (d^2I/dV^2 ($v = 0.5$ V p.p., $s = 0.7$ mm)) remains practically symmetrical also, with one single peak exactly corresponding to the tip of the EDC. The width of this peak is 0.35 eV at mid-height. At higher photon energies, the second derivatives of the EDC's reveal additional features, barely resolved in the EDC's, as seen in Fig. 2(b). In these latter curves, however, all pieces of structure overlap, which results into a generally smooth profile. This, in turn, makes the energy location of a given EDC feature (broad peak or shoulder) relatively inaccurate (within ± 0.3 eV), compared to the classical 0.15 eV over-all resolution. Higher derivation reduces this overlap problem, owing to the narrowing of each individual piece of structure [Fig. 2(a)], and, as a result, reveals a far more richer structure. It will be shown in the next section that a higher derivative spectrum, measured at a given photon energy, may exhibit variations by shifting this energy by less than 100 meV. This being the case, it is expected that spectral features separated by only 100 meV could be differentiated by conveniently reducing slit opening and modulation amplitude.

Two sets of photoemission spectra were obtained from the Te films. The first set deals with α -Te(1) films defined previously. This material was observed to sublimate at temperatures above 430 °K in 10^{-10} -torr vacuum, just as trigonal Te. For this reason, annealing of these films was limited to that temperature. The second set was obtained from Te films first deposited at 100 °K and slowly annealed to 300 °K [α -Te(1)], and then fast cooled to 130 °K. Such films [α -Te(2)] did not sublimate at least up to 480 °K. They were studied between 130 and 480 °K. No photoemission spectra were

measured from Te films deposited at 100 °K and maintained at that temperature.

Trigonal Se was observed to sublime between 330 and 380 °K in a 10^{-10} -torr vacuum. The same occurred on Se films, which were, for that reason, only studied at their deposition temperature, 300 °K.

IV. PHOTOEMISSION RESULTS AND INTERPRETATION

A. Tellurium

1. Photoelectric Threshold

As seen in Sec. II, the kinetic energy of the emitted electrons is directly referred to the surface potential (or vacuum level, E_0). The kinetic energy zero is itself referred to the upper limit of the valence band by measuring the quantum yield of the material and, by extrapolation of this yield, the photoelectric threshold E_T (yield onset), taken to equal the ionization energy or energy difference between the top of the valence band and levels lying about E_0 , or the nearest above it in case this latter stands within a gap separating two conduction bands (as probably the case in Se and Te). The quantum-yield curve obtained from a vacuum-cleaved (10 $\bar{1}0$) face is shown in Fig. 3. Data were corrected for reflection using reflectivity measurements of Tutihasi *et al.*,²⁰ which were obtained at 20° incidence. However, because of the high refraction index and absorption of tellurium (as well as selenium) in the 5–10 eV photon energy range, one may consider³⁵ the reflectance at 45° incidence to be reasonably close to its normal incidence value. From this argument, and considering other sources of experimental uncertainty, the absolute accuracy of these yield measurements is estimated to be about 30% above $h\nu \approx 5.5$ eV, despite their noted good reproducibility ($\pm 5\%$). The early work at higher pressure on polycrystalline Te films by Apker *et al.* have shown higher values, typically of the order of 1×10^{-3} at $h\nu = 6.0$ eV, compared to 2×10^{-4} at the same photon energy in this work.

The value of E_T is usually measured by linearizing the yield (Fowler plot) close to the threshold, using the approximate relation $Y \sim (h\nu - E_T)^n$. A third-power law was tested and is shown in Fig. 3 (inset) to deviate from such a straight-line fit. Recently, Ballantyne³⁶ developed a formalism aiming at describing the energy-dependence of the yield. According to this and considering a rectangular distribution of excited electrons, the yield Y should be proportional to $(h\nu - E_T)^3(h\nu)^{-2}$. Although such a relationship happened to be successfully tested on several materials,³⁷ it failed in the case of trigonal Te, showing no improvement compared to the simple third-power-law fit of Fig. 3 (inset). The reason for this misfit between experiment and Ballantyne's approach could be found in

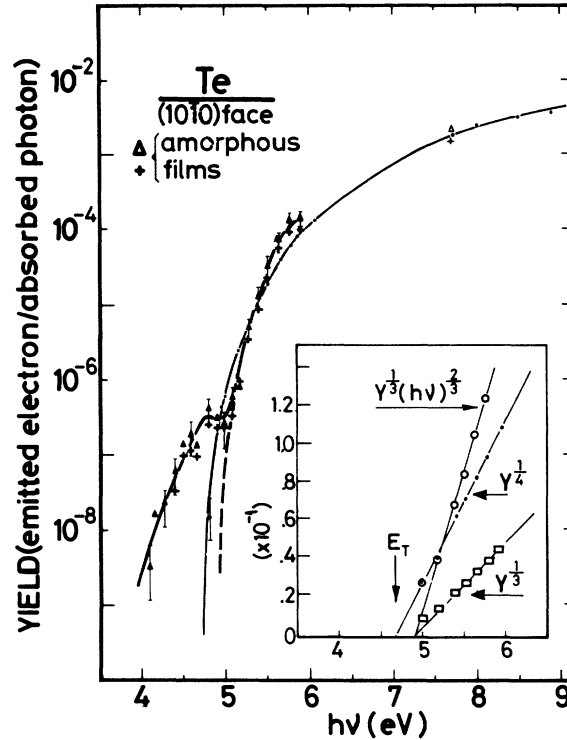


FIG. 3. Photoelectric yield Y of a vacuum cleaved (10 $\bar{1}0$) Te face (\bullet) and of two similarly prepared disordered Te films (Δ , $+$); note the good reproducibility of the latter. In the inset are shown three different power-law fits of the trigonal Te yield; note the straight-line fit of the fourth power law, which gives a photoelectric-threshold (E_T) value of 4.65 ± 0.05 eV.

the fact that, in the latter, no consideration was paid to the case where the vacuum level E_0 lies below the bottom of a conduction band. The best linearization is shown to be obtained for this material using $n=4$, to give $E_T = 4.65 \pm 0.05$ eV. While this value of n agrees with Apker *et al.*,⁴ the photoelectric threshold found in the present work is some 0.25 eV lower than the one found by these authors on films. The present value of E_T is also in concordance with the value obtained directly from the width of the photoelectron EDC's, and was consistently reproduced for all the freshly cleaved faces studied in this work. It agrees furthermore with the one obtained by other workers⁹ from ultra-high-vacuum cleaved tellurium.

According to the calculations of Ref. 1, no conduction-band state would exist at 4.6 eV above valence band edge (Fig. 7 of Ref. 1). However, it is pointed out that the band-structure calculations were performed using pseudopotential form factors fitted to the fundamental band gap between p_2 and p_3 . The precise respective position of each band depends increasingly upon the choice of these form

factors as one moves away from the p_2 - p_3 gap, while the structure of each band is not seriously affected by small variations of the pseudopotential tested. It is therefore expected that the actual location of the SCB is different and most probably lower (to provide for states around 4.6 eV above valence-band edge) than the one shown in Fig. 7 of Ref. 1.

The problem remains as to which level should be set as the bottom of the SCB compared to the top of p_2 . Were the gap between p_3 and the SCB effectively a characteristic of the band structure of Te (as well as of Se²), on line with Ref. 1 and other calculations,³⁶ it would give rise to a "second" absorption edge at the onset of optical transitions between p_2 and SCB, which should be observable experimentally. In this respect, a useful indication is given by the reflectivity data of Tutihasi *et al.*²⁰ In this latter work, the imaginary part of the dielectric constant ϵ_2 and the absorption coefficient α were experimentally determined for trigonal Te. The ϵ_2 and α spectra show distinctively two pieces of structure centered around $h\nu = 5.5$ and 7.5 eV. The first one starts emerging from the background at $h\nu \approx 4.8$ eV and is polarization dependent ($\vec{E} \parallel \vec{c}$). It extends up to $h\nu \approx 6.5$ eV, where the second one takes over. It is remarkable to observe, in contrast, that no structure exists in the two functions considered above, in the photon energy range 3.5–4.8 eV. This would indicate that the actual location of the bottom of the SCB being lower than the one shown in Fig. 7 of Ref. 1, it could not be much lower than 4.8 eV and might therefore correspond to the measured value of the photoelectric threshold, i. e., 4.6–4.7 eV above valence band edge.

As outlined earlier, some uncertainty exists in positioning theoretically not only the SCB but also p_1 . Recent high-energy photoemission measurements on trigonal Te²⁸ set the bottom of p_1 to stand some 5–6 eV below valence band edge, i. e., 1–2 eV lower than the calculated figure (4.0 eV) of Ref. 1. Given a 2-eV width for p_3 , p_1 - p_3 transitions should therefore contribute the optical spectra between $h\nu \sim 2$ and 7–8 eV. If transitions between p_2 and the SCB start contributing about 4.6–4.7 eV, some 3-eV wide overlap is provided between p_1 - p_3 and p_2 -SCB contributions to the optical spectra in the range ~ 4.6 –7.5 eV, in agreement with the general profile of the experimental ϵ_2 spectra.²⁰ The spectral feature mentioned earlier and centered around 5.5 eV lies within this overlap region and one might argue whether this feature could be described by p_1 - p_3 transitions alone. However, the ϵ_2 calculations which were carried out using the band structure of Ref. 1 (see Ref. 3), and which provided a satisfactory structural fit to experimental data as far as the p bands were concerned, do not show any structure at all centered about $h\nu$

= 5.5 eV. Instead, a smooth ramp appears in the theoretical ϵ_2 spectrum extending up to 5.5 eV, where it dies off. Therefore, it does not look probable that this 5.5-eV feature could be associated with p_1 - p_3 but rather with p_2 -SCB transitions.

These arguments give indirect evidence for a second absorption edge in trigonal Te at ~ 4.8 eV, which corresponds to E_T .

Such a parallel between E_T and the onset of optical absorption between p_2 and the SCB might appear to be fortuitous, the vacuum level E_0 lying in this case near the bottom of the SCB. One way to settle this point would be through comparison with other materials characterized by a gap within their conduction band. If there exists a correlation between E_T and a second optical-absorption edge, then a shift of E_T should correspond to any variation of such a gap. As seen in Ref. 1, Se is one of these materials. It will be shown in Sec. IV B 1 that a much larger value of E_T is measured in selenium (6.1 eV), which effectively corresponds (i) to a shift to higher energy of the SCB, according to Sandrock's calculations and Ref. 1 (bottom of the SCB at ~ 6.3 eV above valence band edge), and (ii) to the sharp onset of a ($\vec{E} \parallel \vec{c}$) polarization-dependent peak in the ϵ_2 and α spectra of trigonal Se²³ at photon energies > 6.0 –6.5 eV.

A more detailed study of the photoelectric threshold of trigonal Te is presented elsewhere, which provides additional evidence that the bottom of the SCB lies 4.6–4.7 eV above valence band edge in trigonal Te.

The yield curve of disordered-Te (a -Te) films is shown also in Fig. 3 between 4 and 6 eV. The a -Te reflectivity data used here are those of Stuke and Zimmerer.³⁹ They were obtained from Te films condensed on metallic (Al) substrates maintained at 80 °K, in 10^{-6} -torr vacuum. The preparation of the present Te films being different, one might expect the optical properties of both sets of films to be different as well. However, this would affect the absolute-yield values quoted here only by $\sim 10\%$ to give an overall absolute accuracy of the order of 40% between 5 and 6 eV. This does not affect the general behavior of the yield with photon energy, which was observed to be well reproduced over all the films studied, as exemplified in Fig. 3. In particular, the yield exhibits a pronounced singularity around $h\nu = 5$ eV. Above 5 eV, it follows the yield curve of trigonal Te, and this portion of the curve corresponds to transitions between delocalized states belonging to p_2 and the SCB. Below 5 eV, the a -Te yield curve extends further to lower energy, down to 3.3–3.5 eV, instead of collapsing abruptly around 4.9 eV. This peculiarity of the yield in a -Te curves cannot be associated with contamination (measurements were performed within a few hours after deposition of the films) or

with a reverse current effect,⁴⁰ because of the positive bias (+10 eV) applied to the gold collector during measurement. In addition, this characteristic tailing of the yield correlates with a low-energy tailing observed in energy-distribution curves. Both tailings are not detected in trigonal Te. For these reasons, this portion of the yield curve has been associated with the presence of localized states below the low-energy edge of the second conduction band.⁴¹ These states might be due to chain-end discontinuities and other topological defects in disordered configurations of Te atoms.⁴² It has been observed that the existence and extent of the above-mentioned "tails" do not vary markedly with the thermal treatment of the actual films between 130 and 430 °K. However, this thermal treatment is responsible for variations of the density of states about p_2 , as will be shown later in this section.

The yields were found to be sensitive to contamination under residual gas exposure. In the vacua used in this work, an 0.1 eV down shift of E_T was observed on cleaved (10 $\bar{1}$ 0) Te faces, 3 days after cleaving. This reduced the time available for measurements to about two days on each Te cleaved face. The observed "aging" of Te films was slower, amounting to a 0.1-eV shift five days after preparation of the films.

2. Photoelectron Energy Distribution

Energy-distribution curves (EDC's) and their second derivatives were measured from vacuum-cleaved trigonal-Te (10 $\bar{1}$ 0) faces and from Te films prepared under various conditions. The low-energy onset of all the EDC's (photoelectron kinetic energy zero) is set to equal E_T , thus referring fea-

tures in these EDC's to the top of the valence band on a "final state" energy scale, \mathcal{E} . While this onset (associated with emission from states lying about the bottom of the SCB) is independent of photon energy, the high-energy onset follows exactly the changes in photon energy and traces emission of electrons initially excited from the top of the valence band. The width of each EDC is therefore equal to $(h\nu - E_T)$. Both edges of EDC's were observed to be sharp in trigonal Te. However, only the high-energy onset of the Te films's EDC's were found to be clearly delineated.

a. Trigonal Te. EDC's measured on (10 $\bar{1}$ 0) Te faces are shown in Fig. 4. They were measured under exactly the same experimental conditions (optics and electronic detection) and normalized to the photon input flux. Between $h\nu = 5.9$ and 8.85 eV, the only important spectral feature is the large peak 1.2 eV below the high-energy onset of all the EDC's, which quite certainly delineates a high DOS feature in the valence band. Although finer features exist in these curves, their location cannot be given precisely, even when considering their photon energy dependence. Among these, a shoulder appears at $h\nu = 6.5$ eV [Fig. 4(a)]. It remains at about the same final-state energy position ($\mathcal{E} \approx 5.0$ eV) up to $h\nu = 7.1$ eV, and then disappears. A well-defined peak first emerges on the low-energy side of the 7.72 eV spectrum [Fig. 4(b)]. Its contribution to the EDC increases continuously at higher energies, and simultaneously the profile of the EDC's becomes more asymmetric. This behavior suggests that such a peak could be attributed in part to electron-electron scattering in the bulk.⁴³

Second derivatives of these EDC's are shown in

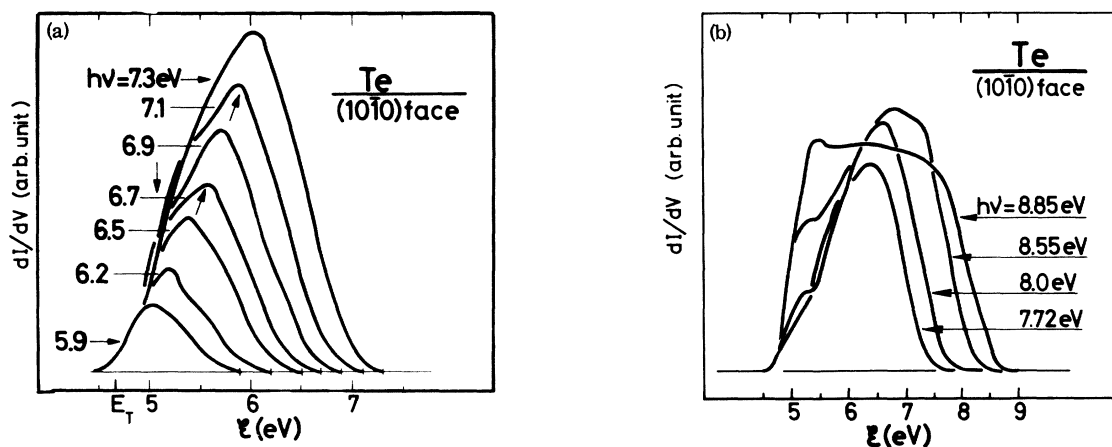


FIG. 4. (a) EDC's measured from a (10 $\bar{1}$ 0) Te face between $h\nu = 5.9$ and 7.3 eV. The evolution of the main peak (arrows) nearly follows photon energy, and a strong shoulder seems to remain fixed at $\mathcal{E} = 5.0$ eV, before weakening at $h\nu = 7.3$ eV. EDC's are normalized to photocurrent. (b) EDC's measured from a (10 $\bar{1}$ 0) Te face between $h\nu = 7.72$ and 8.85 eV. Note the increasing strength of the low-energy peak around $\mathcal{E} = 5.0 - 5.2$ eV. EDC's are normalized to photocurrent.

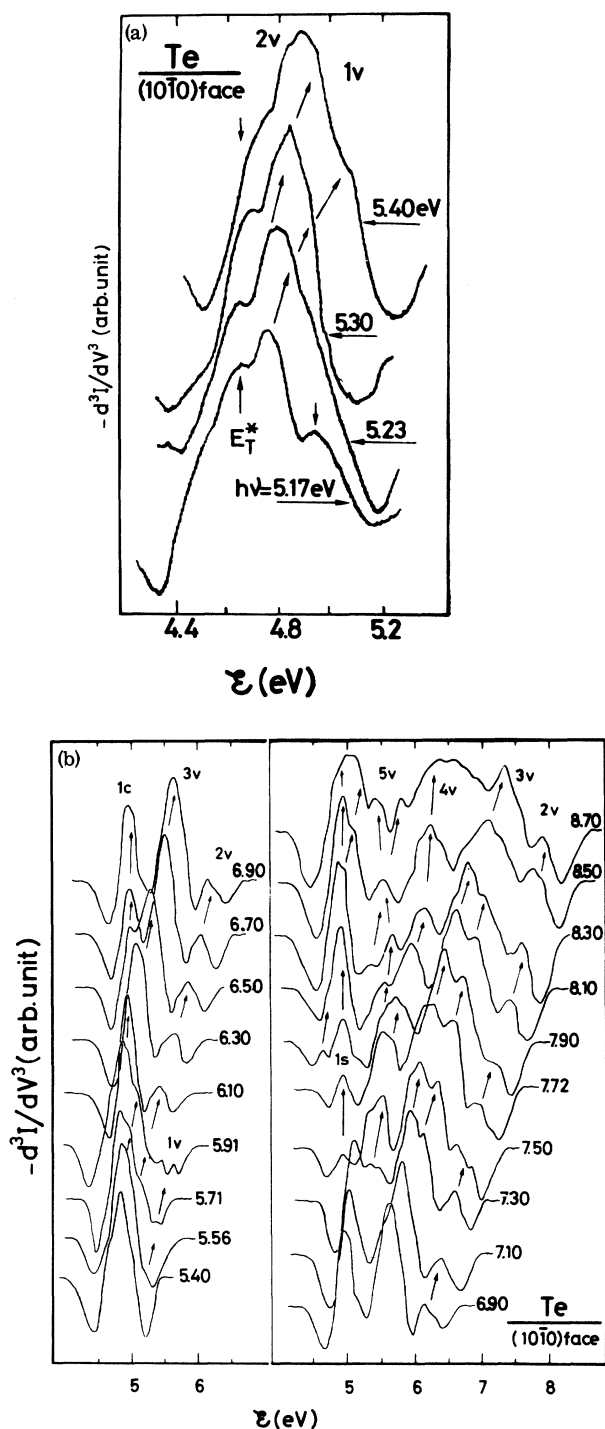


Fig. 5, for photon energies ranging from 5.17 to 8.9 eV. All these curves are normalized to the same maximum vertical amplitude. The signal-to-noise ratio improving rapidly towards low-photon energies, the low-energy spectra exhibit sharp and accurately located peaks. In Fig. 5(a), a first

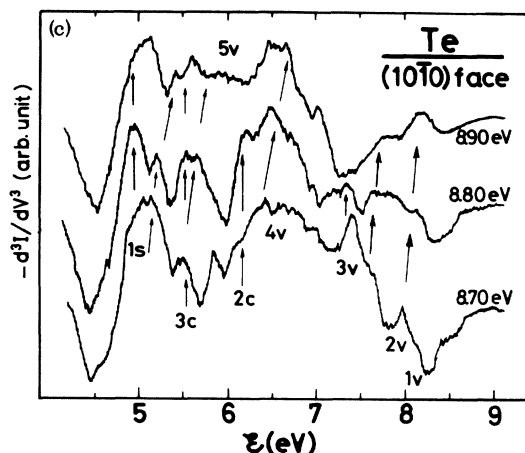


FIG. 5. (a) EDC second derivatives obtained from a $(10\bar{1}0)$ Te face between $h\nu=5.17$ and 5.4 eV. Note the distinct peak at $\mathcal{E}=5.0$ eV, which collapses at higher photon energies. Spectra are normalized to the same maximum vertical magnitude. (b) EDC second-derivatives obtained from a $(10\bar{1}0)$ Te face between $h\nu=5.4$ and 8.7 eV. The evolution of the main features (labeled according to the text) is traced with arrows. Note the splitting of the low-energy peak about $\mathcal{E}=5.1$ eV at $h\nu=6.5$ eV, also the increasing strength of the peak $1s$ above $h\nu=7.5$ eV. Spectra are normalized as in (a). (c) EDC second derivatives obtained from a $(10\bar{1}0)$ Te face between $h\nu=8.7$ and 8.9 eV. Spectra are normalized as in (a).

peak, labeled E_T^* , is detected at $h\nu=4.7$ eV, remaining at that energy before vanishing above $h\nu=5.4$ eV. Although it might be attributed to a fine structure in the DOS near the edge of the SCB, one may remark that its energy location corresponds to E_T . Therefore, it could probably be attributed to the optical-absorption onset between p_2 and the SCB, states lying about the lower edge of the SCB being populated via phonon-assisted transitions in this photon-energy range. Another small peak is observed at $\mathcal{E}=4.95\pm 0.05$ eV on the 5.17-eV spectrum. It seems to weaken at $h\nu=5.23$ eV and disappears at higher photon energies. This behavior over a very short energy range is characteristic of direct transitions which are well localized in the Brillouin zone. These transitions occur here between initial states lying 0.20 – 0.25 eV below valence band edge and final states located about the bottom of the SCB. Such direct transitions cannot be located within the band structure of Fig. 5(a) of Ref. 1. However, a more complete description of this band structure^{13,14} shows that they can only occur about point L , which effectively delineates the bottom of the SCB (Fig. 7 of Ref. 1). This being the case, such a structure could be representative of a M_0 singularity in the joint DOS at the onset of

the direct optical absorption between p_2 and the SCB at point L . The main peak in these spectra remains practically stable at about 4.9 eV before moving upwards above $h\nu = 5.9$ eV. In Fig. 5(b) are displayed the spectra measured between 5.4 and 8.7 eV. Peaks can be traced continuously over the range of energy used. Some of them (labeled 1 to 5 ν) approximately follow the photon energy. At 6.3 eV, the main peak centered at 5.1 eV broadens and further splits at 6.5 eV. As the upper split-off peak (3 ν) follows photon energy and is characteristic of a valence-band DOS feature, the lower split-off peak (1c) will remain at $\mathcal{E} = 5.0$ eV, thus delineating a high conduction-band DOS. Its strength remains constant up to about $h\nu = 7.1$ eV and then collapses at 7.3 eV, when the structure labeled 4 ν arises and moves to higher energies. At 7.5 eV, a small peak appears at about the same energy as 1c. As the excitation energy increases, this peak (1s) gets stronger continuously and is little perturbed by new "valence-band" features moving across it. In Fig. 5(c), three additional spectra measured at 8.7, 8.8, and 8.9 eV are shown. The important point to be stressed here concerns the high-energy section of these spectra. Up to 8.7 eV, the main peaks 1 ν and 3 ν were nearly following the photon energy, though declining in strength above 8.5 eV when compared with 4 ν . At 8.8 eV, these structures weaken considerably and, at 8.9 eV, the dip on the high-energy side of the spectrum seems to be centered at approximately $\mathcal{E} = 7.5$ eV, although its expected position would have been around $\mathcal{E} = 8.5$ eV at $h\nu = 8.9$ eV [on line with the other spectra of Figs. 5(a) and (b)]. This lessening of the high-energy structure (contributed by transitions from the upper part of p_2) corresponds to the observed weakening of the high-energy part of the 8.85 eV EDC, around $\mathcal{E} = 7.5$ –8.0 eV [see Fig. 4(b)]. This is in close agreement with Fig. 6 of Ref. 1, where the calculated DOS of the SCB is shown to weaken markedly some 3.0 eV above the bottom of the SCB, i.e., about $\mathcal{E} = 7.6$ eV. The portion of the 8.9 eV spectrum in Fig. 5(c) between approximately $\mathcal{E} = 7.5$ and 8.9 eV, therefore, corresponds to transitions ending on states lying within the top 1.5-eV wide peak of the DOS of this second conduction band. The next (d -like) conduction band stands just above the SCB with a possible overlap with the latter around 9 eV (as for p_1 and p_2 in the valence band). The low profile of the 8.9 eV spectrum above $\mathcal{E} = 7.5$ eV suggests that such an overlap is probably small. A better picture of this boundary region between the SCB and the next d -like conduction band would certainly have been obtained at higher excitation energies. However, as the photon energy is increased, the peak 1s, which emerges in the 7.5 eV spectrum will tend to overshadow the other features.⁹ This lim-

ited the information which could be collected on the DOS of the material studied in this work. However, as far as the p -valence bands and the SCB are concerned the structure of their density of states can be considered to have been explored conveniently in this work. The low-energy features appearing in the 8.9 eV spectrum of Fig. 5(c) are contributed by transitions initiating some 3.7 eV below valence band edge, i.e., about the bottom of p_1 , and the upper part of the SCB is effectively reached at $h\nu \sim 9.0$ eV with transitions initiating at the top of p_2 .

b. Te films. The energy distributions of photoemitted electrons from Te films prepared under various conditions have been studied and compared with the above-described energy distributions obtained from vacuum-cleaved (10 $\bar{1}0$) Te faces. All Te films studied were deposited in 0.7 – 1×10^{-10} -torr vacuum on silica substrates maintained at 100 °K during condensation of the film, and slowly annealed to room temperature at a rate of $\sim 10^{-1}$ °C/sec. It has been observed that upon further thermal treatment (fast cooling to 130 °K), the profile of the energy-distribution curves of electrons photoemitted from such films could evolve as a consequence of variations in the nature and extent of the short-range ordering present in these thermally strained films, variations which could perturb their electronic structure.

EDC's measured from a Te film first deposited at 100 °K and then heated to 300 °K [a -Te(1)] are shown in Fig. 6 for energies between 7.1 and 8.9 eV. One notes essentially two facts: (i) nearly all features remain stable in initial-state energy scale ($\mathcal{E} - h\nu$), and (ii) the only exception concerns a peak at about $\mathcal{E} \approx 5.0$ eV, which increases in strength continuously as from $h\nu = 7.7$ eV. One may remark also that the low-energy onset of these curves is disturbed by a ramp that does not allow the exact positioning of this onset. While most spectral features seem to delineate structure in the valence-band DOS, a more-detailed investigation is, however, required to clarify the peak on the low-energy region of these EDC's.

The EDC measured on such a film at $h\nu = 7.72$ eV is compared in Fig. 7 with an EDC obtained from a (10 $\bar{1}0$) Te face at the same photon energy. In order to emphasize the energy location of the main peaks, these EDC's were not normalized to the photocurrent, which is expected to vary with the transport mechanisms involved depending on film preparation. At *that* photon energy, the profile of the a -Te(1) EDC is seen not to differ markedly from the trigonal Te EDC, except for the tail appearing on the low-energy side of the a -Te(1) curve. In particular, the two main features at $\mathcal{E} = 5.7$ (shoulder) and 6.3 eV (peak) in the crystalline spectrum are preserved in a -Te(1) in position and

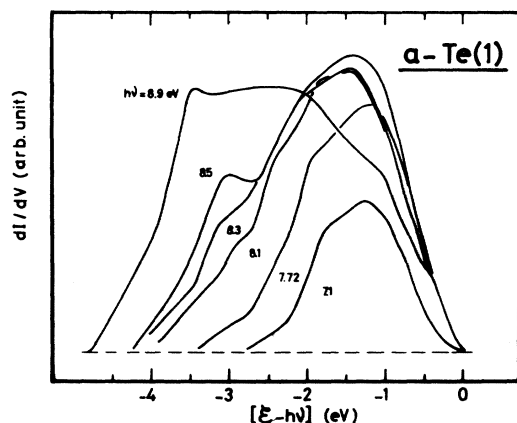


FIG. 6. EDC's measured at 300 °K from a Te film deposited at 100 °K and heated up to 300 °K, in the photon-energy range 7.1–8.9 eV. EDC's are normalized to photocurrent.

relative strength. However, after the *same film* has been cooled rapidly to 130 °K and annealed to 430 °K [*a*-Te(2)], the resulting EDC is shown to be quite different from either the crystalline or the *a*-Te(1) EDC. Although the low-energy tail has been maintained in the *a*-Te(2) EDC, it seems that the shoulder appearing in *a*-Te(1) at 5.7 eV has now evolved into a peak centered around 6.0 eV. The peak at 6.3 eV apparently collapsed into a broad shoulder at approximately the same energy. These observations strongly suggest that *a*-Te(1) and *a*-Te(2) represent probably two quite different disordered configurations of Te atoms.

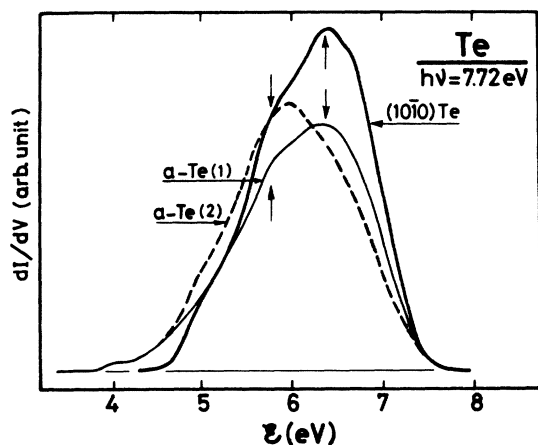


FIG. 7. EDC's measured at $h\nu = 7.72$ eV from a $(10\bar{1}0)$ Te face and from two Te films [*a*-Te(1) and *a*-Te(2)], prepared as explained in the text. Note in the latter the low-energy tailing. These EDC's are not normalized to photocurrent to emphasize the energy location of the main features (at $h\nu = 5.8$ and 6.3 eV).

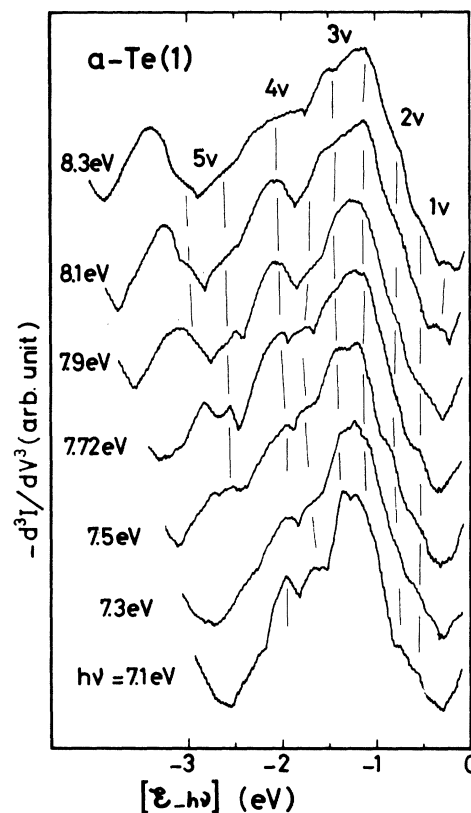


FIG. 8. EDC second derivatives measured from an *a*-Te(1) film, between $h\nu = 7.1$ and 8.3 eV. Labels refer to features identified in the trigonal Te spectra. The spectra are here also normalized as in Fig. 5(a). Spectral features are referred to an "initial state" energy scale ($\mathcal{E} - h\nu$) the zero of which delineates emission from the top of the valence band.

The changes in the profile of these EDC's have been investigated as a function of film preparation using second-derivative spectra. The photon-energy dependence of such spectra obtained from an *a*-Te(1) film is presented in Fig. 8, for energies ranging from $h\nu = 7.1$ eV up to 8.3 eV. The peak position is referred to an initial-state energy scale [$\mathcal{E} - h\nu$], the zero being taken at the top of the crystalline valence band edge, which coincides within 0.1 eV with the upper onset of the photoemission spectra obtained from *a*-Te(1) films, as seen in Fig. 7. Nearly all features (peaks or shoulders) appearing in the spectra of Fig. 8 remain stable in initial-state energy, which indicates that they practically trace the valence-band DOS structure. The only exception is the peak appearing on the low-energy side of these spectra. Its position does not vary on the final-state energy scale (\mathcal{E}) and its strength increases continuously. It could therefore be associated with scattering phenomena, which

could also contribute the peak 1s appearing in the crystalline spectra at $h\nu=7.5$ eV. In a -Te(1), such a structure is shown to be already present in the $h\nu=7.1$ eV spectrum. However, it has been observed that some fluctuation could occur in the appearance of this peak in a manner not clearly understood. It may be remarked that this peak is located at about $\mathcal{E}\approx 5$ eV, i. e., it is contributed by electrons scattered to states lying near the lower edge of the SCB. Such an observation might, therefore, indicate that these states are effectively very sensitive to small variations in the actual ordering present in these films.

As pointed out earlier,^{13,44} the loss of long-range order in atomic configuration should result in a strong smoothing of conduction-band DOS structure. Referring to Fig. 5(b), the sharp conduction band DOS feature 1c is the best detected in higher derivative spectra at $h\nu=7.1$ eV. This spectrum is compared in Fig. 9(a) with different spectra obtained at room temperature (i) from an a -Te(1) film before and after annealing at 430 °K and (ii) from a film deposited at 330 °K on a polycrystalline gold substrate and not annealed to higher temperatures. As in the case of trigonal Te, all these spectra are normalized to the same maximum vertical amplitude. They exhibit small differences which could

hardly be observed on the corresponding EDC's. The absence of the sharp peak 1c in the a -Te(1) spectrum is clearly seen. In addition, the valence-band feature 4v seems to manifest itself more strongly than in the crystal. Upon annealing to 430 °K (limit of sublimation for such films at 10^{-10} torr), 4v decreases in intensity and 1c probably contributes already to the spectrum by pushing the low-energy, positive leading edge of the spectrum to lower energy. On the high-energy side of these two spectra obtained before and after annealing an a -Te(1) film to 430 °K, it is worth noting that the features labeled 1v and 2v in the crystal are present, but much weaker in intensity compared to the crystal. These two features, however, are clearly resolved in the last spectrum, obtained from a film deposited at 330 °K on a polycrystalline gold substrate. In the same spectrum, one may also observe that the crystalline peak (1c) is now almost completely restored in position and strength. However, this spectrum is still different in profile compared to trigonal Te about $\mathcal{E}-h\nu=-1.8$ eV. This suggests that the ordering reached in this film, although close to the trigonal one, is probably slightly disturbed by a certain amount of strain still present in the film. The origin of such small "defects" (chain distortion, fluctuations in bond

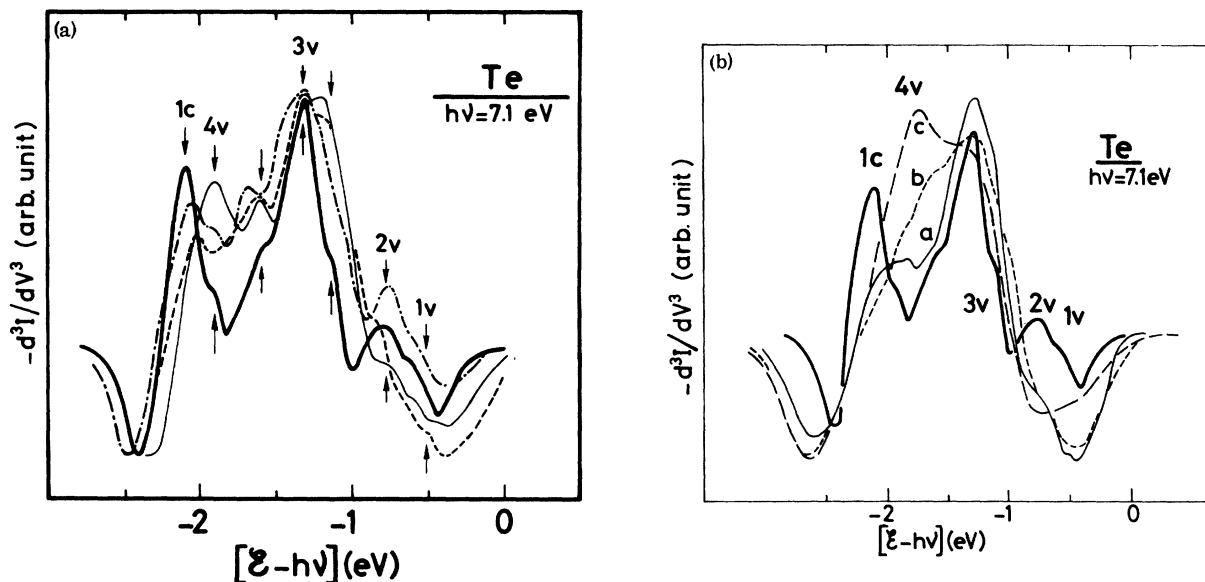


FIG. 9. (a) EDC second derivatives measured at $h\nu=7.1$ eV from (i) a Te film deposited at 100 °K and slowly annealed to 300 °K [a -Te(1), —]; (ii) the same film annealed to 430 °K and slowly cooled to room temperature, (---); (iii) a Te film deposited at 330 °K onto a polycrystalline gold film and slowly cooled to room temperature (---). These spectra are compared to a similar spectrum obtained from trigonal Te (heavy line) [Fig. 6(b)]. Identical settings were used when recording all four spectra. (b) EDC second derivatives measured at $h\nu=7.1$ eV from (a) an a -Te(1) film, (b) rapidly cooled to 130 °K and warmed up to 300 °K and (c) further annealed to 430 °K and cooled to 300 °K. These spectra are compared to a trigonal Te spectrum as in Fig. 9(a) and normalized as in Fig. 5(a). All spectra were measured under the same detection conditions.

length and angles) is probably related to the substrate-film atomic mismatch. Such an effect has been observed to strongly perturb the growth of single-crystal films of Te, grown on a glass substrate.⁴⁵ It has been established that single-crystal Te films having their *c* axis parallel to the substrate have a negligible amount of strain induced by the above mismatch, while that strain is maximum when the films are composed of Te chains perpendicular to the substrate surface. From such a study, one might conclude that stable low-defect Te single-crystal films can only be obtained by minimizing the strain effect mentioned above. Any slight departure from this condition would give rise to lattice distortion. It is clear that such a strain-free situation would be extremely difficult to obtain, so that in most cases Te films probably contain a certain amount of strain.⁴⁶ The magnitude of such a strain in Te films is a matter of conjecture, since no strain measurement has been performed so far in Te films. However, measurements on highly disordered Ge films⁴⁷ yielded a value of 2×10^9 dyn cm⁻² (i. e., 2 ton cm⁻²) which did not disappear upon annealing of the films.

In the *a*-Te(1) film (before annealing to temperatures higher than 300 °K), this disorder is characterized by the lack of conduction band DOS structure and the weaker DOS features at the top of the *p*₂ valence band. Further thermal treatment of *a*-Te(1) films reveals additional variations in the profile of the second-derivative spectra, shown in Figs. 9(b) and 10, which were measured at $h\nu = 7.1$ and 7.72 eV, respectively. As in Fig. 9(a), these curves are normalized to the same maximum vertical amplitude, i. e., practically to the same integrated area. In Fig. 9(b), an *a*-Te(1) film (curve *a*) is first cooled rapidly (~ 1 °C/sec) to 130 °K and slowly annealed to room temperature to yield an *a*-Te(2) film (curve *b*). The valence-band features 1*v* and 2*v* are seen to nearly disappear, while the peak 4*v* (at ~ -2.0 eV) broadens and contributes to a strong shoulder centered around -1.8 eV in the derivative spectrum. The same film is then annealed to 430 °K and cooled rapidly (1 °C/sec) to room temperature. The resulting spectrum (curve *c*) now exhibits three distinct changes. The structure 4*v* has evolved into a peak at $\delta - h\nu = -1.8$ eV. Simultaneously, the peak 3*v* has now weakened and the weak features 1*v* and 2*v* have completely disappeared. This behavior is further confirmed at $h\nu = 7.72$ eV, Fig. 10. At that energy, 1*c* does not show up any more in the trigonal Te spectrum [Fig. 5(b)], but 4*v* is now fully resolved. Curves *a*, *b*, and *c* correspond to the same thermal treatment as curves *a*, *b*, and *c* in Fig. 9(b). The interesting fact here is the inversion of strength between 3*v* and 4*v*. This is seen better in the curve [*c* - *a*] shown in the lower part of the figure, which

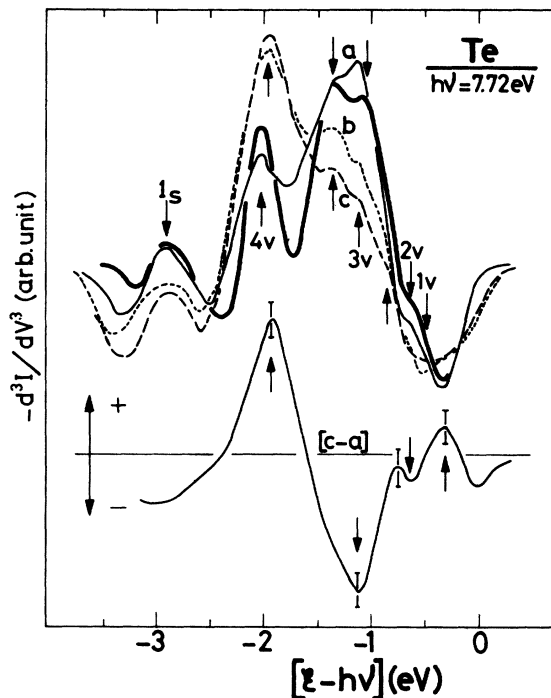


FIG. 10. EDC second derivatives measured at $h\nu = 7.72$ eV from a film prepared under the same sequence as in Fig. 9(b). The lower [*c* - *a*] curve represents the difference between curves *c* [*a*-Te(2)] and *a* [*a*-Te(1)]. Spectra are normalized as in Fig. 5(a), and were obtained using identical instrumental parameters (monochromator slit opening, modulation amplitude, gain, etc.).

represents the intensity difference between curves *c* and *a*. The shift and strengthening of 4*v*, which is observed in Fig. 9(b), is here emphasized, as well as the drop in intensity of 3*v*. One may note, however, that finer structure participating into 3*v* at $\delta - h\nu = -1.4$, -1.1 , and -0.9 eV is still present in the relaxed spectrum (curve *c*). The upper section of curve [*c* - *a*] indicates a dip around -0.6 eV, corresponding to the total loss of 1*v* and 2*v* in curve *c*, but also a small peak centered at -0.3 eV. Associated with the latter is the fact that the negative upper onset of the second-derivative spectrum (curve *c*) has moved upwards in energy by approximately 0.2 eV, compared to curve *a* [*a*-Te(1)] and the crystalline spectrum. Note that the same 0.2 eV shift is observed in curve *b* [obtained after cooling rapidly to 130 °K and slowly warming up to 300 °K an *a*-Te(1) film]. While the high-energy onset of the photoemission spectrum of an *a*-Te(1) film exactly corresponds to the crystalline one, emission of photoelectrons excited from states lying at energies above the valence-band edge of trigonal Te starts contributing the photoemission spectrum after rapidly cooling the

films to 130 °K. The distribution of these states extends ~ 0.2 eV above the trigonal valence band edge, i. e., practically throughout the forbidden band gap of the crystal ($E_G = 0.3$ eV) and corresponds to a shift of 0.2 eV of the Fermi level. A conductivity test was carried out on these Te films that exhibited an *n*-type behavior contrary to trigonal Te or *a*-Te(1). The density of the states above trigonal valence band edge is too small, however, to introduce any important change in the EDC's of Fig. 6. It is revealing that such states arise as soon as the structure of the film departs from the configuration corresponding to *a*-Te(1). This peculiarity at the high-energy edge of curves *b* and *c* of Fig. 10 is also observed in Fig. 9(b), which effectively means that the 0.2 eV tailing mentioned above is representative of a distribution of "initial" states.

The resulting configuration [*a*-Te(2)] thus represents a higher degree of disorder, i. e., a further departure from the trigonal configuration. If such films are once more cooled rapidly to 130 °K and annealed to 430 °K, no further notable change occurs in the spectra, indicating some thermodynamic stability in these Te films that does not exist in the (metastable) *a*-Te(1) films. In addition, it has been observed that such *a*-Te(2) films could be annealed to 480 °K [i. e., above the sublimation limit of trigonal Te and *a*-Te(1) in 10^{-10} -torr vacuum] not only without loss of material, but also without any indication of a reordering mechanism towards a trigonal configuration. This behavior, although not understood, shows that the stability of these films is relatively high. The energy distribution of photoelectrons emitted from *a*-Te(2) films was studied between $h\nu = 6.9$ and 8.1 eV. Within this energy range, no additional information could be obtained concerning the valence-band DOS features of *a*-Te(2) than those quoted above.

c. Energy diagram. A concise way to represent the behavior of features in the energy distributions of photoelectrons is to give the position of these features on a final-state energy scale \mathcal{E} , as a function of the excitation energy $h\nu$. This is done in Fig. 11 in the cases of trigonal Te and *a*-Te(1) films. A more-exact description of the electronic structure of these materials cannot be restricted to the above diagram, where only the energy location of the spectral features is quoted and not their intensity. Therefore, a close comparison has to be drawn between the photon energy dependence of these features both in Fig. 11 and in Fig. 5. In the latter, the relative magnitude of the peaks appearing in the higher-derivative spectra helps significantly in identifying each feature which, therefore, can be traced accurately with photon energy. The lines actually appearing in the energy diagram of Fig. 11 connect points that locate the same spec-

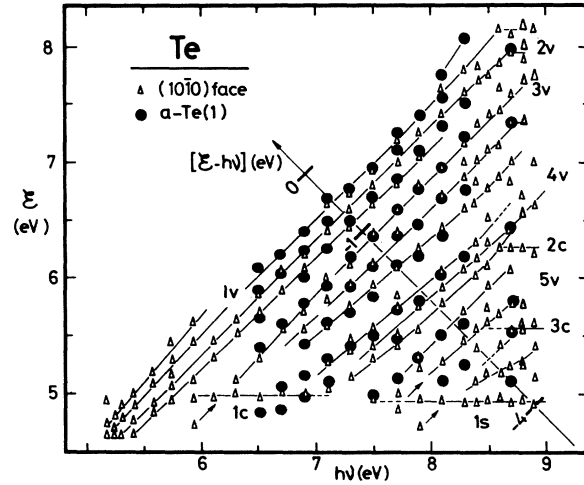


FIG. 11. Energy diagram illustrating the behavior with photon energy of the main spectral features detected in trigonal Te (Δ) and *a*-Te (\bullet) EDC second derivatives. These features can either be referred to a "final-state" energy scale \mathcal{E} , in ordinate or to an "initial-state" energy scale ($\mathcal{E} - h\nu$) on the 45° angle axis across the diagram. Each feature can be traced along a single line, according to its behavior observed in Figs. 5 and 8.

tral features, according to the behavior of these features observed in Fig. 5. Points which might accidentally happen to lie at, say, the same final-state energy but could not be associated with the same spectral feature in Fig. 5, were not connected to each other. Most of the peaks and shoulders detected in the spectra of Fig. 5 are seen to follow the change in photon energy on 45° lines. According to Sec. II, these features, labeled 2*v* to 5*v*, delineate high-DOS regions in p_2 and p_1 . Other points remain stable in the \mathcal{E} scale and delineate high-DOS regions in SCB (1*c* to 3*c*). The peak 1*s*, which remains fixed at $\mathcal{E} \approx 5.0$ eV above $h\nu = 7.5$ eV, has been attributed in part to electron-electron (inelastic) scattering in the bulk. Direct interband transitions also participate at this peak, at least up to $h\nu = 8.3$ eV, as observed from the polarization dependence of the spectra.¹⁴ All the points quoted in this figure have been positioned within experimental uncertainty, i. e., between 50- and 100-meV accuracy. From this energy diagram, DOS features are delineated and their energy location referred to the top of the valence band. This information is then compiled in Table I, where each individual piece of structure is assigned to a portion of the Brillouin zone, according to Fig. 7 of Ref. 1. As mentioned in Sec. II of this paper, a precise assignment of the structure detected in the photoemission spectra would require calculations of the density of photoelectrons [Eq. (1)] as a function of photon energy. However, in the case of Te and Se, where

TABLE I. Energy location and assignment in \vec{k} space of spectral features appearing in the calculated DOS of trigonal and disordered Te (see Fig. 7 of Ref. 1) and in the photoemission spectra obtained from trigonal Te and Te films [α -Te (1)] (see Fig. 11 of this paper). The zero energy is taken at the top of the valence band in crystalline Te. The energy location of the experimental structure can be followed on Figs. 5 and 12. As an example, the features at -2.6 eV appears in the spectra between $h\nu=7.9$ and 8.7 eV, while the one at $+5.0$ eV appears between $h\nu=5.9$ and 7.1 eV. The latter is assigned to emission from states about the bottom of the SCB, at an average energy of 5.0 eV (taking the bottom of the SCB at $\delta=4.6$ eV). Assignment of other features in the experimental spectra is obtained by comparing this structure with partial contributions to the total DOS, which can be *clearly* associated with restricted regions of the Brillouin zone, about point H and along the Δ axis. Features that cannot be attributed to transitions occurring within any of these small volumes in \vec{k} space are associated with the rest of the Brillouin zone, $BZ - (\Delta + H)$, or with the whole Brillouin zone (BZ). Labeling of the structure is the same as in Fig. 11.

TRIGONAL Te			α -Te(1)			
THEORY (eV)	EXP. (eV)	ASSIGNMENT	THEORY (eV)	EXP. (eV)	ASSIGNMENT	STRUCTURE
- 3.6	- 3.4 \pm 0.2	H				
- 3.3		BZ - Δ				
- 3.1	- 3.1 \pm 0.1	BZ - Δ	- 3.1	- 3.1 \pm 0.1	BZ - Δ	5v
- 2.9	- 2.9 \pm 0.1	BZ	- 2.6	- 2.6 \pm 0.1	Δ	
- 2.5	- 2.6 \pm 0.1	BZ - H	- 2.5	- 2.6 \pm 0.1	BZ - H	4v
- 2.4	- 2.35 \pm 0.1	Δ	- 2.15	- 2.1 \pm 0.1	Δ	
- 2.2	- 2.15 \pm 0.1	Δ				
- 2.0	- 2.0 \pm 0.1	Δ	- 1.85	- 1.75 \pm 0.1	Δ	
- 1.7	- 1.7 \pm 0.1	BZ - ($\Delta + H$)				
- 1.5		BZ - ($\Delta + H$)	- 1.5	- 1.45 \pm 0.1	BZ - ($H + \Delta$)	3v
- 1.3	- 1.35 \pm 0.1	BZ - ($\Delta + H$)	- 1.1	- 1.15 \pm 0.05	Δ	
- 1.1	- 1.15 \pm 0.1	Δ, H				
- 0.9	- 0.85 \pm 0.05	Δ, H				
- 0.7	- 0.7 \pm 0.05	Δ	- 0.8	- 0.8 \pm 0.05	Δ	2v
- 0.5	- 0.5 \pm 0.05	BZ	- 0.5	- 0.5 \pm 0.05	Δ	
- 0.2	- 0.3 \pm 0.05	H	- 0.25	- 0.25 \pm 0.1	H	1v
4.8	5.0 \pm 0.1	BZ - ($\Delta + H$)	—	—		1c
5.7	5.6 \pm 0.15	BZ - ($\Delta + H$)	—	—		3c
6.05		Δ	—	—		
6.2	6.3 \pm 0.15	BZ - H	—	—		2c

large portions of the bands remain constant in energy, such calculations may not be necessary in order to assign EDC features to peaks or shoulders in the valence-band or conduction-band total DOS. Because higher-derivative techniques emphasize primarily the energy location of these EDC features, weak spectral features can be revealed, and their energy location compared with partial contributions to the total DOS, originating in some high-symmetry regions of the Brillouin zone, in particular around point H and along the Δ axis. With these considerations in mind, the agreement between the theoretical and experimental locations of trigonal Te DOS features is seen to be particularly good in the valence band, but less accurate in the conduction band. This uncertainty deals with the difficulty encountered in adjusting the values of the pseudopotential (see Ref. 1) in order to find a correct positioning of valence or conduction bands lying away from the p_2 - p_3 forbidden-band gap. As said earlier, the fit between theory and experiment is obtained by shifting the calculated second conduction band (SCB) by 1.2 eV to lower energy.

The α -Te(1) valence-band features are shown to be very close to those of the crystal, at least in position. The assignment of these DOS features,

which are not drastically affected by the loss of long-range order, should be the same as the assignment of identical crystalline features in the complex-band-structure approach (Ref. 1). This concerns essentially the valence-band DOS extending more than 1 eV below the valence band edge. Just below this edge, however (peaks $1v$ and $2v$), a weakening of the relevant structure has been observed (Fig. 9). Such a behavior was effectively predicted in the DOS calculations of Ref. 1 to occur upon disordering the trigonal configuration. In Fig. 12(a) the crystalline and disordered DOS spectra of p_2 (Fig. 7 of Ref. 1) are superimposed to emphasize the detailed nature of the changes occurring within this band upon disorder, i.e., when increasing α . It is clearly seen here that the two main peaks at ~ -0.4 eV (corresponding to $1v$) and ~ -1.0 eV ($2v$) weaken, and that $1v$ (the closest to valence band edge) is the most affected by this weakening. One may also notice that the contribution of point H extends from the valence band edge down to -1.7 eV, i.e., in the range of energy primarily perturbed at this stage of disorder [α -Te(1)]. This point H contribution is maximum at ~ -0.4 eV, i.e., around the spectral feature $1v$. Upon disorder ($\alpha=0.13$, for instance), this con-

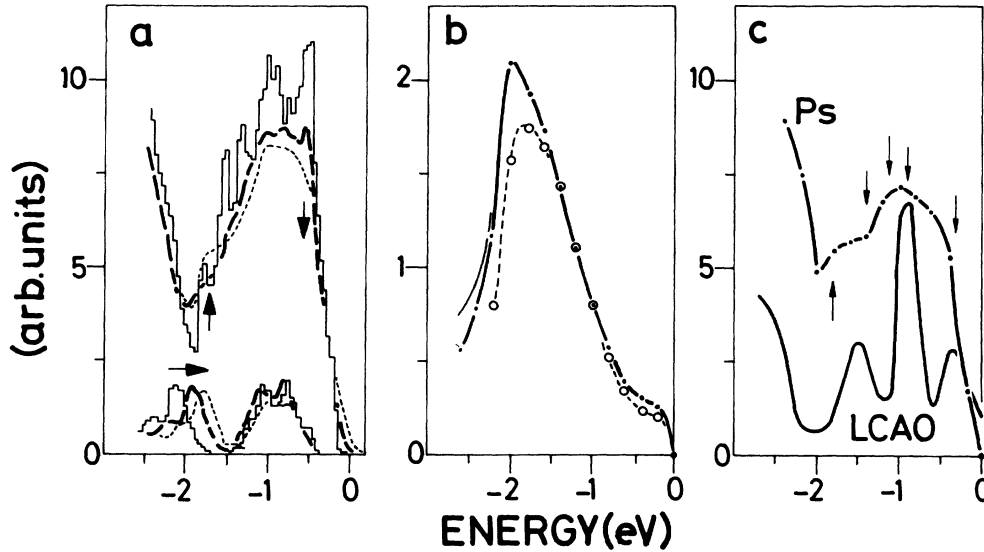


FIG. 12. (a) Density-of-states variations at the top of the Te valence band upon increasing α [$\alpha=0$, histogram; $\alpha=0.11$, --; $\alpha=0.13$, - . -] from Fig. 7 of Ref. 1. At the bottom of the figure is shown the evolution of the Δ contribution of this valence-band DOS for the three values of α . Note the shift to higher energy of the p_1 Δ contribution (maximum at -2.1 eV for $\alpha=0$), which moves into the p_2 total DOS. To this shift corresponds an increase of the total DOS at -1.8 eV (arrows). Simultaneously, the Δ contribution of the p_2 DOS does not vary significantly. The sharp decreases observed about -0.5 eV are due to the weakening of the H contribution to the p_2 DOS, which is not shown in this figure for clarity (see Fig. 7 of Ref. 1). (b) Evolution with initial-state energy ($\xi - \hbar\nu$, zero at the top of the valence band) of the function $A\xi(\xi) |\mathcal{N}_w|^2$ derived, as explained in the text, from two a -Te(1) EDC's measured at 7.72 (heavy line) and 7.1 eV (---) and using the valence-band DOS of Fig. 12(a), at $\alpha=0.11$. The fit between these two curves is good down to -1.5 eV ($\xi=5.6$ eV), where the 7.1 eV curve starts to collapse, owing to the effect of the escape function $\xi(\xi)$. This effect is transferred to the 7.72 eV curve, which is then corrected (thin line) below -2.1 eV ($\xi=5.6$ eV), to show the behavior of $|\mathcal{N}_w|^2$ alone. (c) Semiexperimental DOS at the top of the valence band in a -Te(2), as deduced from an a -Te(2) EDC measured at 7.72 eV (Fig. 7 of this paper), and using the function $A\xi(\xi) |\mathcal{N}_w|^2$ of Fig. 12(b), as explained in the text (- . -). The integrated DOS, between 0 and -2.4 eV, has been arbitrarily set to equal the integrated DOS obtained for $\alpha=0.11$ [Fig. 12(a)], in order to emphasize the structural variation of the p_2 DOS between a -Te(1) and a -Te(2). LCAO calculations (Ref. 49) performed on a disordered Te network are shown for comparison (—). Arrows refer to the experimental spectral features of Fig. 10.

tribution loses some 50% of its intensity, which affects the total DOS around -0.4 eV. If one takes the observed weakening of 1ν to be associated with this decrease in the H contribution, this, in turn, suggests that this region of the Brillouin zone is particularly sensitive to disorder. The same parallel between Figs 9 and 12(a) can be drawn concerning 2ν (~ -1.0 eV). The contribution from the Δ -symmetry axis is in this case much larger than that from H . Thus, the decrease in strength of 2ν (Fig. 9) could be due to disorder affecting point H as well as the Δ axis. However, a clearer idea of the effect of disorder on the Δ symmetry alone is obtained when considering the total distribution of states about -2.0 eV, i.e., in the region where p_1 and p_2 overlap. As seen in Fig. 7 of Ref. 1, point H does not contribute to the total DOS in the range -1.7 to -2.6 eV. Upon increasing α , the dip located at -2.0 eV in the crystal is first seen to fill up ($\alpha=0.11$) and a new peak appears at -1.8 eV ($\alpha=0.13$), which did not show up clearly at

$\alpha=0.11$. The evolution of that region of the DOS can be entirely ascribed to the Δ axis as seen in the lower part of the figure. The Δ contribution to the total DOS, which delineates the upper part of p_1 in the crystal, moves upwards to -1.9 eV ($\alpha=0.11$) and -1.8 eV ($\alpha=0.13$) without losing its strength. This causes the appearance of a new peak at -1.8 eV in the disordered material, which is in fact representative of a deeper overlap between p_1 and p_2 upon disorder. This being the case, however, Figs. 7 and 9(b) show that 4ν is practically identical in relative strength and location in both trigonal Te and a -Te(1) films, although the piece of structure ($1\nu+2\nu$) is different in both configurations. This suggests that the disorder present in a -Te(1) films does not yet affect the energy levels of the states belonging to the Δ -symmetry axis in the Brillouin zone of Te. Since the symmetry of this axis corresponds to the hexagonal (c) axis in real space, i.e., to the axis about which the Te atoms are helically distributed, the above observa-

tions might be interpreted by saying that the actual short-range ordering in a -Te(1) could be very close to the one present in trigonal Te along the c axis.

This interpretation of the data is based on the density-of-states calculations presented in Ref. 1. Whatever their inherent limitations, these calculations indicate *trends* in the way perturbation of the trigonal Te configuration could affect its electronic structure. Probably, the most interesting point concerns the behavior of the Δ contribution to the total DOS upon increasing α . Such a contribution should move upwards when accentuating the disorder, i. e., upon perturbing, not the long-range order (which is seen to vanish for low values of α without affecting the valence-band DOS), but the short-range order. This being the case, introducing strain effects into the a -Te(1) films and, therefore, further perturbing the ordering present in these films, should result in (i) an additional weakening of the total DOS in the upper section of p_2 , and (ii) a strengthening of the photoemission spectra about $\mathcal{E} - h\nu = -1.8$ eV. Although the validity of the approach described in Ref. 1 is not expected to hold for large degrees of disorder, the above trends should be reasonably predicted.

The behavior of a -Te(1) upon additional thermal treatment leading to a -Te(2) films seems to confirm these views. As seen in Fig. 10, 4ν moves from -2.1 to -1.8 eV with a very strong increase in strength. Simultaneously, 3ν collapses and $(1\nu + 2\nu)$ disappears completely. These effects are probably due to a strong perturbation occurring in the *nature* of the short-range ordering of these films upon fast cooling to 130°K and subsequent heating to 300°K . While these effects were predictable qualitatively, their magnitude seems to be too large to be described by the theoretical approach presented in Ref. 1, even for large values of the disorder parameter α . However, an optical density of states of a -Te(2) can be obtained by deconvoluting the a -Te(2) EDC of Fig. 8, as follows. Taking the \vec{k} -conservation law to be relaxed in amorphous materials, one may derive from Eq. (1) an approximate energy distribution of electrons propagating into an amorphous solid and photoemitted in vacuum by

$$N(\mathcal{E}, h\nu) = A\xi(\mathcal{E})n_v(\mathcal{E} - h\nu)n_c(\mathcal{E})|\mathfrak{M}_{vc}|^2. \quad (7)$$

The contribution of scattered electrons to the measured EDC can be considered to be negligible at low-photon energies, so that the electron-electron scattering function has been omitted in this expression.⁴⁸ A is a normalizing constant and $\xi(\mathcal{E})$ is the probability for an electron to be emitted in vacuum without undergoing inelastic scattering in the bulk. The "average" oscillator strength \mathfrak{M}_{vc} couples initial and final states lying at energies $(\mathcal{E} - h\nu)$ and \mathcal{E} , respectively. It may vary with the actual wave

functions of these states and, therefore, the effective matrix elements $|\mathfrak{M}_{vc}|^2$ may present variations with energy. The valence-band DOS $n_v(\mathcal{E} - h\nu)$ and the conduction-band DOS $n_c(\mathcal{E})$ of a -Te(1) are taken to equal the respective values of the density of states calculated with $\alpha=0.11$, (Fig. 7 of Ref. 1). Dividing the actually measured energy distribution $N'(\mathcal{E}, h\nu=7.72$ eV) by the combined valence-conduction-bands DOS $[n_v(\mathcal{E} - 7.72)n_c(\mathcal{E})]$ yields a function [Fig. 12(b)] that corresponds to the product $A\xi(\mathcal{E})|\mathfrak{M}_{vc}|^2$. In order to evaluate the influence of $\xi(\mathcal{E})$ alone over this function, a similar calculation was carried out for an a -Te(1) EDC measured at $h\nu=7.1$ eV. The result [dashed curve, Fig. 12(b)] indicates, that the escape probability $\xi(\mathcal{E})$ starts disturbing the spectra at about $\mathcal{E} - 7.1 = -1.5$ eV, i. e., around $\mathcal{E}=5.6$ eV. Transferring this indication to the curve obtained at 7.72 eV shows that the profile of this curve might represent reasonably well the energy dependence of the effective matrix elements, averaged over the whole Brillouin zone, within the complex band-structure approximation (Ref. 1) for transitions initiating within the top 2.1 eV of the p_2 valence band. Assuming, thus, that (i) the energy dependence of both $|\mathfrak{M}_{vc}|^2$ and $\xi(\mathcal{E})$ to be the same in a -Te(1) and a -Te(2), and (ii) the DOS of the second conduction band to be nearly constant in a -Te(2), as expected from the DOS profile obtained with $\alpha=0.13$ (Fig. 7 of Ref. 1), one can deconvolute the combined valence-conduction band DOS of a -Te(2) from the a -Te(2) EDC (Fig. 8), and, furthermore, the profile of the a -Te(2) valence-band DOS between -2.4 and 0 eV. The result (P_s), based on the pseudopotential calculations [Fig. 12(a)], is shown in Fig. 12(c). Within the above assumptions, one might consider the resulting curve to describe reasonably well the actual characteristics of the p_2 DOS in a -Te(2), as it confirms the predicted evolution of this region of the total DOS upon increasing α [Fig. 12(a)]. However, a direct theoretical fit to this experimental p_2 DOS using the proposed model (Ref. 1) would have required large values of α (≥ 0.15), so that the actual atomic network of a -Te(2) might barely recall the original trigonal Te lattice ($\alpha=0$). In Fig. 12(c), a comparison is drawn between the present a -Te(2) extrapolated p_2 DOS and the one obtained by Hartmann and Mahanti⁴⁹ using a tight-binding [linear-combination-of-atomic-orbitals (LCAO)] method. While the energy location of the three peaks delineating the p_2 band in this approach seems to correspond with the observed experimental structure, one may remark, however, that the width of these peaks does not agree with the experiment. If such a p_2 DOS profile would have been effective, all three peaks would have been easily resolved, within experimental error, without using higher-derivative techniques. Instead, the actual

data seem to support the pseudopotential approach in Ref. 1.

To summarize, the electronic structure of α -Te(1) films has been observed to evolve upon fast cooling and subsequent annealing in such a way that:

(i) the p_1 and p_2 valence bands now overlap strongly, due to the shift to higher energy of the Δ contribution to the p_1 DOS, and

(ii) the H contribution to the p_2 DOS is practically absent in the α -Te(2) spectra, and the p_2 DOS itself has weakened considerably compared to the p_1 DOS.

These facts could indicate that, while α -Te(1) was probably made of a mixture of small nearly-undistorted helical chains, the strain effect induced by fast cooling introduces strong variations in the bond angles. It could, therefore, be responsible for distortion of these small chains to a point where the short-range ordering present in α -Te(2) could be associated with a crystalline structure, different from the trigonal configuration. This possibility will be discussed in the last section of this paper. No diffraction studies were carried out on these films. These could possibly have brought some light into this domain, anticipating translational symmetry to be restored in the films upon annealing.

B. Selenium

1. Photoelectric Threshold

The quantum-yield curve of vacuum-cleaved (10 $\bar{1}0$) Se faces (Fig. 13) has been obtained using the reflectivity data of Leiga.²³ The reproducibility of these yield data ($\pm 10\%$) was not observed to be as good as that experienced with trigonal Te, owing to the lower quality of the cleaving performed on the Se crystals. The only yield measurements performed so far on trigonal Se are those of Tredgold *et al.*⁷ They indicate a threshold of 4.2–4.3 eV, in disagreement with the present data. It has been observed in this work that such a threshold value is characteristic of contaminated trigonal Se, *before* cleaving in vacuum of the order of 7×10^{-11} torr. Around $h\nu = 6.0$ –6.1 eV the present yield curve shows nonmonotonicity. This peculiarity cannot be attributed to a negative (reverse) current effect for the same reason that was mentioned for the Te films, and because of contamination by residual gas, which results in a shift of the lower edge of the EDC's. Such a shift was observed to be as large as 0.25 eV three days after cleaving but was negligible during the first 24 hours, during which measurements were made. The presence of this yield tail made an extrapolation of the photoelectric threshold for this material difficult. Different attempts were made to linearize this yield. The results are shown in the inset in Fig. 13.

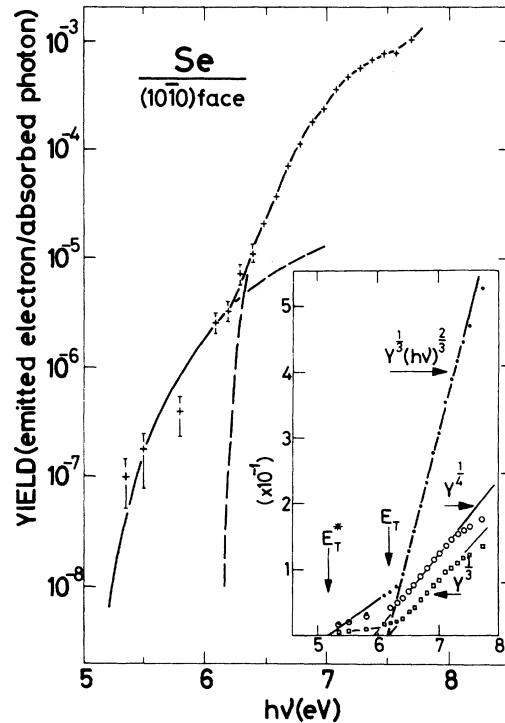


FIG. 13. Photoelectric yield Y of a vacuum cleaved (10 $\bar{1}0$) Se face. Three different power-law fits to this yield curve are shown in the inset. Straight-line extrapolation of $Y^{1/4}$ gives a threshold at 5.95 eV, while the two other functions give a value of about 6.15 eV. The actual value of E_T is taken to average these three figures to 6.1 ± 0.2 eV. Below 6.2 eV, all three functions show nonlinearity extending down to ≈ 5.2 eV (E_T^*). The two straight lines going through the $Y^{1/3}(h\nu)^{2/3}$ points are only intended to be representative of the fit experienced using any of the three simple functions. They are transferred to the yield curve below 6.5 eV, where the observed poor fit to experimental points indicates that the actual mechanism responsible for the yield tail is quite probably complex.

Contrary to trigonal Te, the fourth-power law of $Y(h\nu)$ does not seem here to yield any reasonable straight-line fit above $h\nu = 6.2$ eV as well as Balantyne's proportionality and the third-power law. Below 6.2 eV, none of the Y -vs- $h\nu$ proportionality relationships succeed also in eliminating the nonmonotonic behavior. The resulting tailing of the yield could probably extend down to 5–5.2 eV, which delineates a photoelectric threshold E_T^* . By extrapolating the three tested straight-line fits to zero, one obtains an average value of $E_T = 6.1 \pm 0.2$ eV. In view of the density-of-states spectrum of Se near the upper limit of p_2 and at the bottom of the SCB (Fig. 8 of Ref. 1), it is quite unlikely that the yield behavior between 5.0 and 6.2 eV could be associated with band-structure details. The value of E_T , however, does compare well with the cal-

culated energy separation (≈ 6.3 eV) between p_2 and the SCB (Fig. 8 of Ref. 1). In this respect, it is worth noting that optical-absorption data obtained from trigonal Se were, in particular, very well reproduced theoretically²⁴ in this region of the photon energy spectrum by using the band-structure calculations presented in Ref. 1. In particular, a peak begins to emerge in the ϵ_2 spectrum²³ of trigonal Se at $h\nu = 6.0$ – 6.5 eV, which can only be attributed to p_2 –SCB transitions. It seems, therefore, very reasonable to assign the value of E_T to the onset of optical absorption between p_2 and SCB, as has been done for trigonal Te. On the other hand, if such a nonmonotonicity exists in the yield, it should correspond to a certain contribution in the energy distribution of the photoemitted electrons. It will be shown below that, for $h\nu \leq 6.5$ eV, EDC's are increasingly affected by the emission of electrons excited from initial states lying within the forbidden band gap, i. e., up to 1–1.5 eV above valence-band edge. Notwithstanding the possibility of a tail of localized states existing below the SCB in Se, which might account for the observed yield tail (although the s character of this band should preclude such a possibility⁴²), there is strong evidence for the existence of gap states above p_2 in the trigonal Se crystals used.⁵⁰ This being the case, explanations for the presence of such states could be found by considering either the impurity content or the lattice defects of these crystals. The latter were strongly thallium-doped to $\sim 10^{20}$ atom/cm³. At that level of doping, it seems clear that (Th) impurity states should appear in the band gap in sufficient density as to affect the optical properties of the material.⁵¹ Electrons, after being trapped on these states, could be detrapped by absorption of a photon and excited towards the SCB states. On the other hand, such crystals may probably present a relatively high density of crystalline defects. These defects could be located at the surface. Being associated with the few fibres still present along the cleaved plane of the sample, they could be characterized by a density of unsatisfied ("dangling") bonds.⁵² The density of bulk-lattice defects can be expected to be comparatively much larger. Localized levels caused by these defects could be populated via localized excitonic processes accompanied by the absorption of phonons.⁵³ Such processes have been tested to describe quite well the strong absorption tail observed in trigonal Se¹⁷ and could possibly be responsible for the photoluminescence properties of this material.⁵⁴ It is believed that all the above considerations contribute simultaneously to the interpretation of the observed yield tail in trigonal Se. Such a yield behavior has also been observed in nearly degenerate semiconductors⁵⁵ and nonstoichiometric compounds, like PbSe and PbTe.⁵⁶

As far as the electronic structure of Se is concerned, one may consider the energy difference between p_2 and SCB to be experimentally measured at 6.1 ± 0.2 eV. In this respect, the large difference between the values of E_T obtained for trigonal Se and trigonal Te does not appear to be attributable to the respective surface potentials of these parent materials, but rather to the respective positions of their second conduction band, i. e., to the presence of a gap between p_3 and SCB.

The profile of the yield curve of disordered Se films prepared from the same Se crystals as above was found to resemble the one obtained from trigonal Se, the only change being a possible shift of E_T to 6.2–6.3 eV, in agreement with Nielsen's measurements.¹⁰ The loss of long-range order in a -Se films⁵⁷ is further expected to perturb even more⁵⁸ the nature and extent of the gap states evidenced in trigonal Se. As far as "aging" problems were concerned, the amorphous phase happened to be more stable than its crystalline counterpart, as in Te, with working time extending over three days without any detectable contamination effect, as observed by tracing the energy location of the low-energy edge of EDC's at mid-height. This remark on the "stability" of a -Se would somewhat agree with similar observations on a -Se films prepared under various conditions by Leiga.⁸ However, the present yield figures seem to be two to three times smaller than the ones found by this author. The film preparation could explain the difference. The films used by Leiga were prepared by deposition on a clean brass substrate maintained at 60 °C, in a vacuum of the order of 10^{-4} torr, and then transferred to a different vacuum system for photoemission study.

2. Photoelectron Energy Distribution

a. Trigonal Se. EDC's and their second derivatives were measured from trigonal Se in the range $h\nu = 6.0$ – 10.5 eV. As an example, an EDC from trigonal Se measured at 7.72 eV is shown in Fig. 14(a). At that photon energy, the gap-states emission is less than 1% of the total emission,⁵⁹ so that the tailing above the high-energy edge of the EDC does not show up on this curve. This allows the EDC to be positioned on the \mathcal{E} scale by extrapolating this edge to zero and taking the resulting "onset" of the curve to equal $h\nu$. On the low-energy edge, the actual EDC exhibits some tailing that is attributed to reverse negative-current effect introduced by scattered light after reflection from imperfections in the cleaved faces. The main body of the spectrum consists essentially of one peak pointing at 7.0–7.2 eV. No other feature manifests itself, despite the optimized parameters used to measure this EDC (0.2-mm slits and 70-mV-p. p. modulation). The evolution of such a curve between $h\nu = 6.8$ and

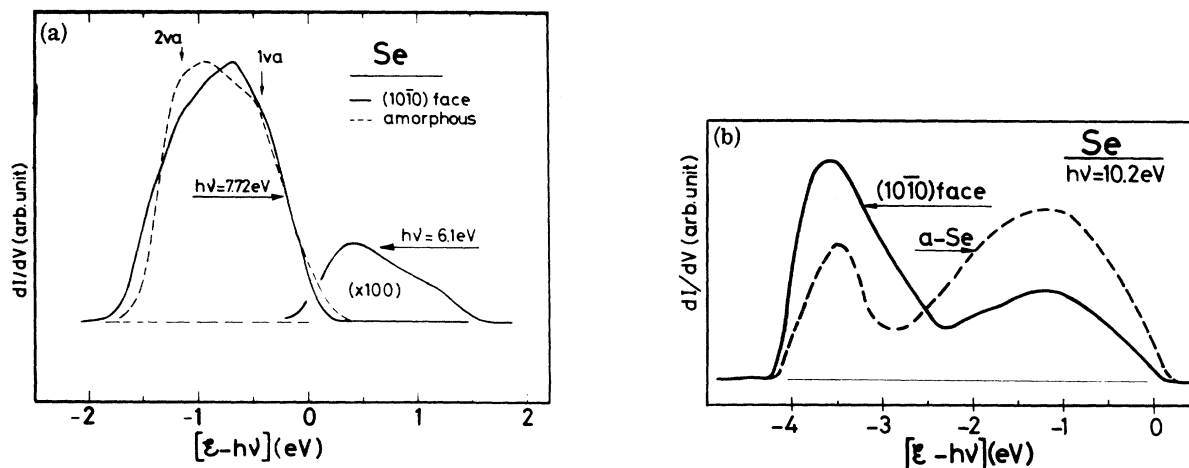


FIG. 14. (a) EDC's measured from (1010) Se (—), at $h\nu = 7.72$ and 6.1 eV, and from an amorphous Se film, at $h\nu = 7.72$ eV (---). Note the two features (1va and 2va) appearing in the amorphous Se EDC, in contrast with the 7.72 eV EDC of trigonal Se. (b) EDC's measured at $h\nu = 10.2$ eV from (1010) Se (this work) and an amorphous Se film (Ref. 10). The curves are not normalized to photocurrent. The high-energy peak, centered at $\xi - h\nu = -1.2$ eV, is relatively stronger than the low-energy peak around -3.5 eV in *a*-Se, in striking contrast with the relative strength of these two peaks in trigonal Se.

8.5 eV does not yield any clear information on the DOS structure present in these curves, which consist in general of weak, transient shoulders superimposed on a broad peak centered at about the middle of each spectrum, as in Fig. 14(a). Below 6.8 eV the high-energy tailing becomes increasingly prominent. The EDC measured at 6.1 eV is shown in Fig. 14(a) to be some 1.5 eV wide, extending up to about $\xi = 7.5$ – 7.7 eV. Such a distribution of electrons could be representative of the profile of the actual density of the initial "gap" states involved in the photoemission process, at $h\nu = 6.1$ eV. However, as pointed out earlier, the nature of these states is most probably complex. For this reason, no attempt is made here at defining a hypothetical "optical" density of these gap states, as is often done in the literature, assuming the drift mobilities of propagating and tunneling electrons to be the same.⁴⁸ Above $h\nu = 9.0$ – 9.2 eV, emission from p_1 begins to emerge in the spectra, as shown in Fig. 14(b).

Higher derivative techniques were extremely useful in revealing the fine structure embedded in the trigonal Se EDC's. The spectra recorded between $h\nu = 7.1$ and 8.5 eV are presented in Fig. 15(a). These Se spectra are seen to evolve much more rapidly with photon energy than those of Te (Fig. 5). This behavior is a direct consequence of the larger dispersion of the Se bands as compared to Te. As a result, the structure of the Se photoelectron-energy distributions, which is here better described by the joint DOS (\vec{k} conservation) rather than the crude combined DOS (energy conservation), is much more sensitive to photon-energy

changes than the Te structure, in which large portions of bands are nearly \vec{k} independent, i.e., where the combined-DOS picture applies more readily (see Sec. II). This remark would preclude in general direct identification of features of the valence or conduction-band DOS in the Se photoemission spectra over an extended photon energy range, as has been done for Te. On the other hand, while the intensity of the spectra in the high-energy region remains relatively small, the low-energy edge raises very steeply. As observed in Fig. 8 of Ref. 1, the p_2 DOS remains low down to about -0.7 eV and increases abruptly below that level. This behavior is well supported by the profile of the upper 1 eV of the photoemission spectra. On the other hand, the SCB DOS in Fig. 8 of Ref. 1 does not seem to increase rapidly enough to describe the sharp increase in the spectra around $\xi = 6.1$ eV. While the presence of such a spectral feature is not unexpected at that energy (onset of optical absorption between p_2 and the SCB at $E_T = 6.1$ eV), it is probable that electron surface scattering due to the presence of a large number of crystalline imperfections at the surface could occur, and could result in an enhancement of the low-energy region of the photoemission spectra, next to E_T .⁵⁵ This explanation would seem to be reasonable in view of the fact that second-derivative spectra measured at the same photon energy but from different cleaved faces have shown slight variations of the steepness of this edge.

Among features appearing in the higher-derivative spectra, some behave like "valence-band" or "conduction-band" DOS features, over a short pho-

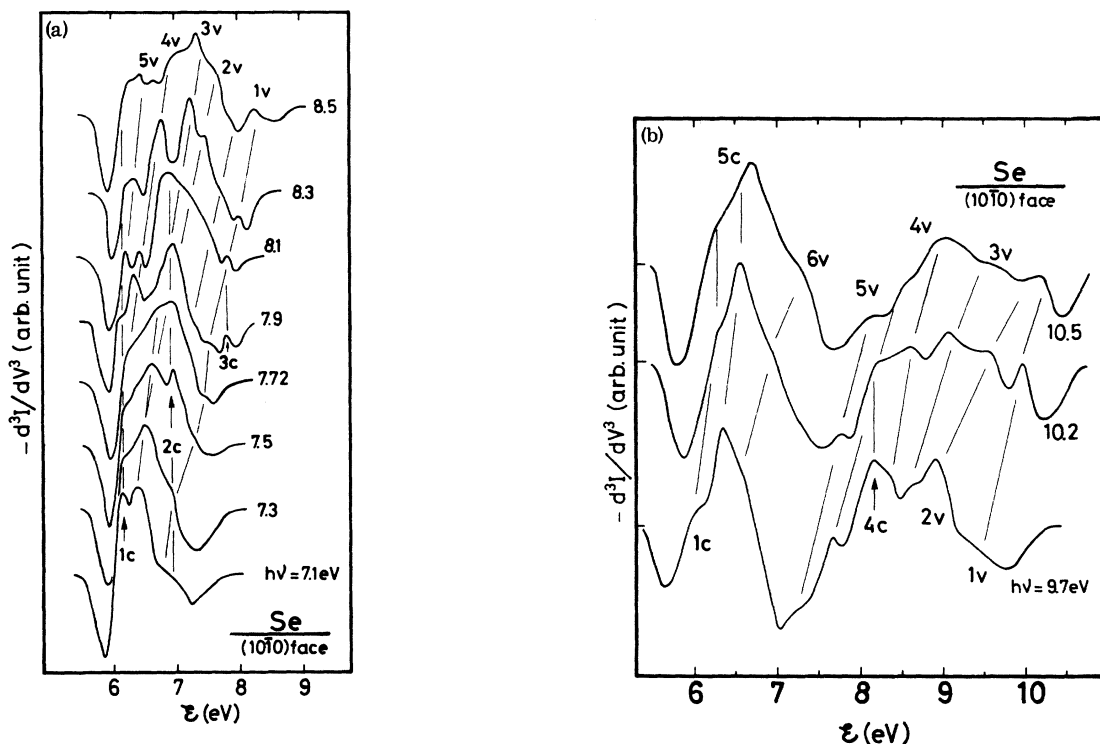


FIG. 15. (a) EDC second derivatives measured from $(10\bar{1}0)$ Se between $h\nu=7.1$ and 8.5 eV. Labels refer to spectral features related to either conduction ($1c$ to $3c$) or valence band ($1v$ to $5v$) DOS features. Spectra are normalized as in Fig. 5(a). (b) EDC second derivatives measured from $(10\bar{1}0)$ Se at $h\nu=9.7$, 10.2 , and 10.5 eV.

ton-energy range. They are labeled $1v$ to $5v$ and $1c$ to $4c$, respectively. The strongest structure is the peak $2c$ at $\epsilon=6.9$ eV, which seems to emerge already at $h\nu=7.1$ eV and persists in the spectra up to $h\nu=8.1$ eV. It corresponds to the only peak apparent on the EDC of Fig. 14(a). It delineates a conduction-band DOS feature which seems to correspond to the sharp peak of the SCB DOS located some 7.1 eV above valence-band edge (Fig. 8 of Ref. 1) and contributed by most of the Brillouin zone except H and Δ . The strength of the latter peak is, however, larger than the strength of $2c$. Additional derivative spectra measured at $h\nu=9.7$, 10.2 , and 10.5 eV are shown in Fig. 15(b). As expected from Fig. 8 of Ref. 1, emission from p_1 is now apparent and starts around $\epsilon - h\nu = -2.8$ eV, in agreement with Fig. 14(b). At $h\nu=10.5$ eV, the low-energy section of the spectrum is probably contributed by the large peak located in the upper part of the p_1 DOS and centered at $\epsilon - h\nu = -3.8$ eV, as seen in Fig. 8 of Ref. 1. In all these spectra, the same shoulder $1c$ observed in Fig. 15(a) appears again. Emission initiated at states belonging to p_2 extends over nearly 3 eV in the higher-energy part of these spectra, in agreement with the calculated width of this band, as seen in Fig. 8 of Ref. 1. The only spectral feature which

could be associated with a high-conduction-band DOS lies about $\epsilon=8.1$ eV in the two lower spectra of Fig. 14(b). The corresponding feature in the DOS of the SCB (Fig. 8 of Ref. 1) is probably the second strongest peak in that band centered about 8.3 eV. For these transitions, initial states lie between -1.6 and -2.1 eV, at $h\nu=9.7$ and 10.2 eV, respectively, i. e., within the 1-eV wide peak centered about the middle of p_2 . These two DOS features in p_2 and the SCB are equally contributed by the whole Brillouin zone.

b. Disordered Se. A series of EDC's were obtained from disordered Se (a -Se) films prepared as described in Sec. III. Owing to the high vapor pressure of this element, annealing treatments were precluded, so that the disordered-to-crystalline transition could not be explored here as it was done for a -Te films. An EDC obtained at $h\nu=7.72$ eV from an as-deposited film is shown in Fig. 14(a). As in the case of trigonal Se, a tailing appears on the high-energy edge of the spectrum. The low-energy edge is extrapolated to about $6.1-6.2$ eV. The main body of the EDC distinctly shows two features at $\epsilon=6.5$ and 7.2 eV that are not apparent on the trigonal Se EDC. In Fig. 14(b), a trigonal Se EDC measured at 10.2 eV is compared with an EDC measured at the same photon energy

from an α -Se film prepared by Nielsen¹⁰ in a manner very similar to the one used in this work, except for substrate choice. With this in mind, one might consider the main features of the electronic structures of both series of films to be in reasonably good concordance. By comparing this spectrum to the trigonal Se spectrum, it is seen that the p_1 contribution to the EDC's seems to be twice smaller in α -Se than in trigonal Se, compared to the p_2 contribution. Reasons for this discrepancy could be found either in the trigonal Se or α -Se electronic structure. In view of the fact that the relative strength of the p_1 emission in α -Se is in good agreement with the calculated p_1 DOS (Fig. 8 of Ref. 1), it is probable that electron scattering in the imperfectly grown and cleaved Se crystals could be responsible for the increased strength of the low-energy portion of the crystalline spectrum. In addition, the matrix elements could be effectively larger for p_1 -SCB than for p_2 -SCB transitions in trigonal Se, as confirmed by the trigonal Se ϵ_2 calculations of Sandrook,²⁴ in the 10–12-eV photon energy range. On the other hand, disorder could also affect these matrix elements and reduce the p_1 contribution to the measured α -Se EDC's. Second-derivative spectra are displayed in Fig. 16.

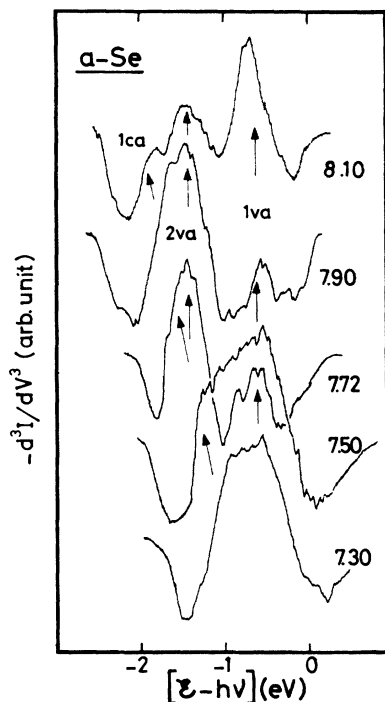


FIG. 16. EDC second derivatives measured from α -Se between $h\nu=7.3$ and 8.1 eV. Peaks remaining stable in the initial-state energy scale delineate features in the p_2 valence-band DOS. Note the distinct peak (1ca) resolved at 8.1 eV, around $\epsilon - h\nu = -1.8$ eV ($\epsilon = 6.3$ eV).

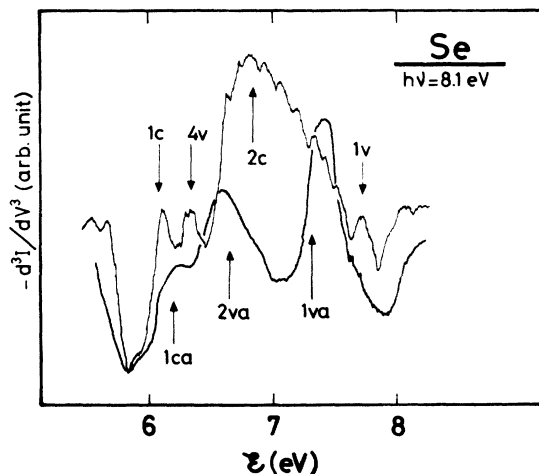


FIG. 17. Comparison between two EDC second derivatives measured at the same photon energy $h\nu=8.1$ eV, from trigonal Se and α -Se. Note the sharp dip present in the α -Se spectrum around $\epsilon=7$ eV, in contrast with the crystalline spectrum.

They were measured between $h\nu=7.3$ and 8.1 eV, i. e., in the range where the strong-peak 2c representative of a high-conduction-band DOS manifests itself in the crystalline spectra. It is seen that upon increasing $h\nu$, the peaks 1va and 2va are progressively dissociated, and that a small feature (1ca) remains fixed on the low-energy side of the spectra. The two first peaks are characteristic of features of the valence-band DOS, lying at -0.7 and -1.5 eV below the crystalline valence band edge, respectively. The last feature (1ca) could either be associated with a weak structure still present in the conduction-band DOS, as obtained in Fig. 7 of Ref. 1 at $\alpha=0.075$, or with inelastic scattering in the bulk of the film. The striking feature in these spectra is the total absence of peak 2c, which completely overshadows the valence-band features 2v and 3v in the crystal, as emphasized in Fig. 17, for $h\nu=8.1$ eV.

The present α -Se spectra exhibited some variations over a series of films prepared under similar conditions. These variations essentially affected the relative strengths of 1va and 2va. In all situations, however, the peak 2c was not observed in the spectra. This behavior is indicative of fluctuations in the nature of the short-range ordering, long-range order being completely lacking. Here again, it appears that, unless all the preparation conditions are precisely controlled, reproducibility of the details of the electronic structure cannot, in general, be achieved systematically. From this point of view, a comparison between data obtained from films prepared in different manners could only show a partial agreement, limited essentially,

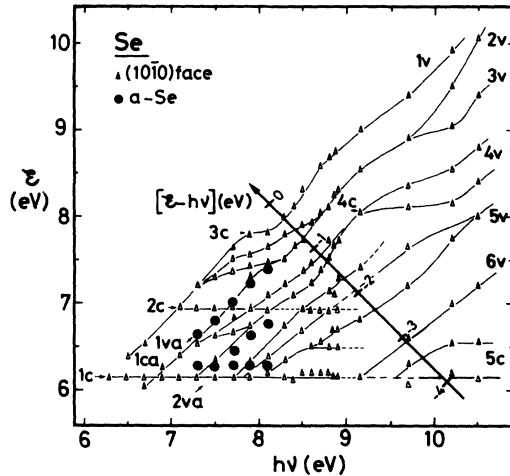


FIG. 18. Energy diagram similar to Fig. 11, in the case of trigonal Se (Δ) and *a*-Se (\bullet).

in the case of *a*-Se, to the near disappearance of conduction-band structure.

c. Energy diagram. The spectral features detected in second-derivative spectra of trigonal and amorphous Se are presented on the energy diagram of Fig. 18, in a way similar to Fig. 11. The lines joining points associated with the same spectral feature intersect in a complex manner, which is characteristic of direct transitions. Peak 1c is seen to appear continuously over the whole photon-energy range studied. Structure 2c emerges at $h\nu = 7.1$ eV, disappears at 8.3 eV and reappears

again at 8.5 eV up to 8.9 eV. Along this range, initial states from which electrons are excited towards SCB levels about $\mathcal{E} = 7.0$ eV are lying (i) very close to the top of p_2 ($h\nu = 7.0 - 7.2$ eV), i. e., at point *H*, and in this case could be excited directly to states around *H*, at $\mathcal{E} = 7.1$ eV; (ii) deeper in p_2 ($7.5 < h\nu < 8.1$ eV) and practically scattered all over the Brillouin zone, between $\mathcal{E} - h\nu = -0.05$ and -1.1 eV, i. e., about the high DOS features labeled 2*v* and 3*v*; (iii) between -1.4 and -1.8 eV ($8.5 < h\nu < 8.9$ eV), i. e., in the high DOS region of p_2 corresponding to 4*v* and contributed by the entire Brillouin zone. The next conduction-band features 3*c* and 4*c* are transient features which might be associated with excitations around the Δ axis and point *H*, initial states lying about $\mathcal{E} - h\nu = -0.7$ and -0.2 eV, respectively. The relatively strong peak 5*c* at $\mathcal{E} = 8.1$ eV emerges around $h\nu \approx 9.0$ eV and can be traced up to 10 eV, i. e., initial states lie between -1.0 and -2.0 eV approximately, in a region where *H* and Δ contribute negligibly to the total DOS.

The energy positions of these experimentally detected DOS features are compared in Table II with features appearing in the calculated DOS of Fig. 8 of Ref. 1. Their assignment to particular regions of the Brillouin zone has been obtained as in Te. Among the three high DOS features observed in *a*-Se and labeled 1*ca*, 1*va*, and 2*va*, the conduction-band feature 1*ca* is located about $\mathcal{E} = 6.3$ eV. From a comparison with Figs. 6 and 8 of Ref. 1, it might be associated with the lower portion of the SCB, which is contributed by slices 4 and 5 of the Brillouin zone containing points Γ and *K* (Fig. 4 of

TABLE II. Energy location and assignment in \vec{k} space of spectral features appearing in the calculated DOS of trigonal and disordered Se (Fig. 8 of Ref. 1) and in the photoemission spectra obtained from trigonal Se and amorphous Se films (Fig. 18 of this paper). Note that, contrary to tellurium, several experimental features quoted in this table are distinctly observed only over a small photon energy range, as seen in Fig. 18. This is typically the case for the conduction band feature 3*c* at $\mathcal{E} = 7.8$ eV, which is observed only for $7.9 \leq h\nu \leq 8.1$ eV and corresponds to transitions about most of the Brillouin zone except *H*. Other assignments are carried out as for Te in Table I.

TRIGONAL Se				AMORPHOUS Se			
THEORY (eV)	EXP. (eV)	ASSIGNMENT	STRUCTURE	THEORY (eV)	EXP. (eV)	ASSIGNMENT	STRUCTURE
-3.4	-3.4 ± 0.1						
-3.1	-3.1 ± 0.1	BZ - ($\Delta + H$)	6 <i>v</i>				
-2.5	-2.5 ± 0.1	BZ					
-2.0	-2.1 ± 0.1	BZ - ($\Delta + H$)	5 <i>v</i>				
-1.8	-1.8 ± 0.1	BZ					
-1.6	-1.6 ± 0.1	BZ - ($\Delta + H$)	4 <i>v</i>				
-1.2	-1.2 ± 0.1	H, Δ					
-1.0	-1.0 ± 0.1	BZ - ($\Delta + H$)	3 <i>v</i>	1.4	-1.3 ± 0.2	Δ	2 <i>va</i>
-0.7	-0.7 ± 0.1	Δ	2 <i>v</i>	0.65	-0.7 ± 0.2	Δ	1 <i>va</i>
-0.2	0.2 ± 0.1	H	1 <i>v</i>				
6.2	6.2 ± 0.1	K, L	1 <i>c</i>	6.6	6.3 ± 0.2	K, L	1 <i>ca</i>
6.6	6.6 ± 0.1	BZ - ($\Delta + H$)	5 <i>c</i>				
7.2	7.0 ± 0.1	BZ	2 <i>c</i>				
7.8	7.8 ± 0.2	BZ - H	3 <i>c</i>				
8.3	8.1 ± 0.3	H, Δ	4 <i>c</i>				

Ref. 1). The preservation of such conduction-band structure in *a*-Se contrasts with the total absence of structure in the SCB of disordered Te (Fig. 7 of Ref. 1). The valence-band DOS features $1va$ and $2va$ are approximately located at -0.7 and -1.3 eV, respectively, and correspond to the partial contribution of the Δ axis in the total DOS (Fig. 8 of Ref. 1). In contrast, it is interesting to note the absence of any structure between 0 and -0.5 eV in the case of *a*-Se. In this region of the crystalline DOS, the excitation processes initiate almost completely about point *H*. Therefore, it appears that the disorder primarily affects the *H* contribution to the total p_2 DOS, while its Δ contribution is preserved. This behavior has also been observed in *a*-Te(1) and might correspond to the persistence of small helical chain of Se atoms in this form of disordered Se.⁶⁰

In a manner similar to what has been done in the case of *a*-Te(1), it appeared interesting to evaluate the function $A\xi(\mathcal{E})|\mathfrak{M}_{vc}|^2$ for *a*-Se. The energy distribution measured at $h\nu = 7.72$ eV [Fig. 14(a)] was used as well as the densities of states n_v and n_c calculated with $\alpha = 0.075$ (Fig. 8 of Ref. 1). The result is shown in Fig. 19. Below $\mathcal{E} - h\nu = -1$ eV (or below $\mathcal{E} \approx 6.7$ eV), the above function is seen to increase markedly, suggesting that the escape-probability function $\xi(\mathcal{E})$ does not yet seriously affect the energy distributions for final states

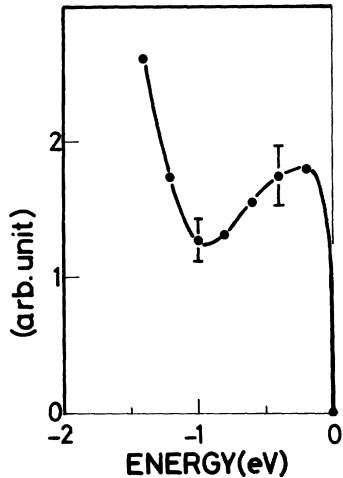


FIG. 19. Variation of the $A\xi(\mathcal{E})|\mathfrak{M}_{vc}|^2$ function, with initial-state energy ($\mathcal{E} - h\nu$), derived from an *a*-Se EDC measured at 7.72 eV [Fig. 14(a)] and using the valence-band DOS of Fig. 8 of Ref. 1, at $\alpha = 0.075$. The sharp increase of that function below -1.0 eV indicates that $\xi(\mathcal{E})$ does not significantly effect this function, at least down to $\mathcal{E} - h\nu \approx -1.2$ eV, i. e., $\mathcal{E} \approx 6.5$ eV, or just a few tenths of an eV above the actual E_T value of 6.1 ± 0.2 eV. This observation correlates a similar behavior observed in *a*-Te(1) [see Fig. 12(b)].

lying as low as 0.4 – 0.5 eV above the photoelectric threshold of 6.1 eV. On the other hand, the average matrix elements $|\mathfrak{M}_{vc}|^2$ are shown to vary depending on the initial-state energy level.² This behavior confirms a similar observation on *a*-Te(1) [Fig. 12(b)]. It indicates that matrix-element variations should be taken explicitly into account when evaluating the EDC's of *a*-Se, as well as of *a*-Te, in contrast with current approximations allowing these matrix elements to be constant over a several-eV wide energy range.¹⁰

V. AMORPHOUS VERSUS CRYSTALLINE ATOMIC-CONFIGURATION CHARACTERISTICS OF TELLURIUM AND SELENIUM

Starting from the trigonal configurations of Te and Se, the disorder effects can be summarized as follows:

(i) The conduction-band structure of both materials seem to be more strongly affected by disorder than the valence bands. This leads to a completely structureless conduction-band DOS in the case of Te, whereas some residual structure seems to persist in Se, in agreement with disorder effects described within the model proposed in Ref. 1.

(ii) In addition, the valence-band DOS of *a*-Te(1) and *a*-Se show some departure from the crystalline DOS, owing to the lack of long-range order. Comparing the experimental results (Tables I and II) with the calculated DOS, it appears that, even for large values of α (≥ 0.11 in Te and ≥ 0.07 in Se), the only DOS features persisting in the valence band are those which are associated with the DOS partial contribution from the \vec{k} -space region around the Δ axis.

(iii) As a consequence, the best fits to the experimental *a*-Te(1) and *a*-Se spectra are obtained by choosing $\alpha \approx 0.11$ and 0.075 , respectively. Defining the diameter of the short-range order region by $\Delta = a_0/\alpha$ (where a_0 is the next-nearest-neighbor distance), one obtains $\Delta = 9a_0$ and $13a_0$ for *a*-Te(1) and *a*-Se, respectively. These estimates correspond to weakly distorted chains containing about 10 [*a*-Te(1)] and 14 [*a*-Se] atoms. The above figures are not, of course, expected to give a complete description of the structural properties of these disordered films, which can be complicated by the occurrence of other atomic configurations (like, for instance, Se_8 rings in the case of *a*-Se⁶¹). However, they might be taken as roughly characterizing the disorder present in these films.⁶²

(iv) In *a*-Te(2) films, one observes a large increase in the part of the photoemission spectrum associated with the bottom of p_2 and the top of p_1 (-1.5 to -2.0 eV), whereas its high-energy part (top of p_2) loses considerable strength, as compared to *a*-Te(1). On the other hand, as it appears

in Fig. 8 of Ref. 1 ($\alpha = 0.13$) and in Fig. 12(a), the Δ contribution to the p_1 band is shifted to higher energy, giving rise to a peak in the low-energy part of p_2 . Simultaneously, the high-energy part of p_2 is weakened, owing to a larger broadening affecting the energy bands, particularly near point H . Although the proposed theoretical approximation is expected to break down for large values of α ,¹ this result indicates qualitatively the correct trend along which the electronic structure of more disordered configurations of Te atoms may evolve.

To obtain an insight into the structural properties of disordered Te and Se films, it appears then necessary to reconsider the atomic distribution functions presented in Figs. 3(a) and 3(b) of Ref. 1. In the case of Se, an experimental atomic-distribution curve is available.⁶³ From the comparison of this curve with the theoretical curve obtained for $\alpha = 0.07$, one concludes that their agreement is good up to the third-nearest neighbors (beside a shift in second-nearest-neighbor distances). The peak corresponding to the fourth- and fifth-nearest neighbors is contributed by atoms belonging to adjacent chains. This peak is very weak in the experimental curve and cannot be reproduced theoretically using a constant value of α . It appears then that discrepancies between the theoretical and experimental curves of Se always occur when the contributing atoms belong to different chains. Since the present photoemission data on α -Se are explained reasonably well by the proposed model,¹ it might be concluded that the DOS features detected in the energy range covered by the present work are mainly determined by interactions between atoms belonging to the same chain. However, because the bond length in trigonal and monoclinic Se are quite similar, rings and chains cannot be distinguished by considering only the radial distribution functions. Therefore, the occurrence of a certain amount of ring configurations mixed with small chains cannot be excluded in the α -Se films studied in this work. Such a mixed configuration has been envisaged by other authors^{11,61} to explain the electronic properties of similarly prepared films, labeled as α -SeII by Richter.⁶⁴ A clear answer to this problem would be to investigate the electronic structure of monoclinic Se. Unfortunately, (i) the instability of this material renders its photoemission study practically impossible⁶⁵ and (ii) theoretical pseudopotential calculations of its band structure are far too complicated to be envisaged, owing to the large number of atoms present in the unit cell of monoclinic Se.

In the case of Te, the only experimental radial-distribution-function study available⁶⁶ has been carried out on 100- to 150-Å thick Te films deposited onto a Polyvinyl-Formvar substrate held at liquid-He temperature in 10^{-6} -torr vacuum. Such films

were observed to crystallize upon heating at 23 °C. The actual preparation of the films used in this work are very different, and one may not expect their characteristics to be similar to the former ones. Effectively, the present films did not show any evidence of "crystallization" at room temperature, and before annealing to higher temperatures, by x-ray diffraction. However, the study referred to above does show that the Te films analyzed are still probably made of small (~ 10 atoms) chains interconnected in a complex manner.

As far as the present films are concerned, some conclusions can be drawn from the behavior of the calculated distribution with increasing α [Fig. 3(a) of Ref. 1]. For small α values (< 0.09), the peaks belonging to the first- and second-nearest neighbors are well separated. For higher values of α (> 0.13), these two peaks merge into an average structure centered about 3.1 Å. The resulting total number of atoms contributing to that average peak is *six*. The third- and fourth-nearest neighbors in the disordered ($\alpha > 0.13$) trigonal configuration merge into a single broad peak at about 4.7 Å, contributed then by a total of *twelve* atoms. These (average) *six* first-nearest and *twelve* second-nearest neighbors are exactly the coordination numbers of a *simple cubic* lattice. So, while α -Te(1) appears to be *quantitatively* well described by using the disordered-trigonal-configuration approach ($\alpha = 0.11$), i. e., consisting essentially of small nearly undistorted helical chains, α -Te(2) could be described only *qualitatively* by increasing the disorder parameter α above 0.13. Considering the atomic distribution function for $\alpha = 0.13$ [Fig. 3(a) of Ref. 1], it leads to the assumption that α -Te(2) may contain a majority of simple cubic coordinated atoms. As a consequence, the α -Te(2) electronic structure might be more accurately described by introducing disorder into a simple cubic Te lattice, instead of a trigonal one. These conclusions concerning the simple cubic approach to the α -Te(2) configuration seem to correlate the observations of Tourand and Breuil,⁶⁷ who determined the radial distribution function of liquid Te at different temperatures, using neutron diffraction. In this particular case of disorder, the bond angle is seen to decrease continuously when increasing the temperature, from 103° in trigonal Te to 94° at 1725 °C. Furthermore, at that temperature, the (100) diffraction ray appears in the reciprocal lattice, giving evidence for a simple cubic α -Pononium-like structure. It may be expected that such an evolution of the Te configuration towards a simple cubic lattice could also be obtained by stressing trigonal Te under very high pressures.⁶⁸

In the light of these investigations, it appears that some of the questions which arose during the course of this work still remain open. It would be

interesting to measure, for instance, the atomic distribution function of trigonal and disordered Te, particularly with regard to the α -Te(2) modification. Moreover, it would be valuable to perform a calculation of the band structure and density of states of simple cubic Te, and extend this calculation to the case of a disordered cubic Te model. These particular calculations are in progress and will be published in a future paper.

ACKNOWLEDGMENTS

The authors are grateful to Dr. B. Fitton for stimulating discussions and for his encouragement

during the course of this work. They would also like to thank the following people for their informative comments and access to results prior to publication: Professor P. H. Cutler and Professor J. Stuke, and Dr. M. Anderegg, Dr. B. Feuerbacher, Dr. R. C. Keezer, Dr. A. A. Lucas, Dr. P. Nielsen, Dr. R. Pinchaux, Dr. G. Tourand, Dr. R. F. Willis, and Dr. G. Zimmerer. The assistance and technical expertise of M. R. Barnes in performing the measurements are gratefully acknowledged. Two of us (B. K. and K. M.) are indebted to the Deutsche Forschungsgemeinschaft for financial support.

- ¹B. Kramer, K. Maschke, and L. D. Laude, preceding paper, Phys. Rev. B **8**, 5781 (1973).
- ²R. Sandrock, Phys. Rev. B **169**, 642 (1968).
- ³K. Maschke, Phys. Status Solidi **47**, 511 (1971).
- ⁴L. Apker, E. Taft, and J. Dickey, Phys. Rev. **74**, 1462 (1948); E. Taft and L. Apker, J. Opt. Soc. Am. **43**, 81 (1953).
- ⁵W. Pong and R. A. Norris, J. Opt. Soc. Am. **55**, 1189 (1965).
- ⁶H. Merdy, Ann. Phys. (Paris) **1**, 289 (1966).
- ⁷R. H. Tredgold, R. H. Williams, G. Kavalyauskene, and R. Keezer, Phys. Status Solidi **26**, K5 (1968).
- ⁸A. G. Leiga, J. Appl. Phys. **41**, 3227 (1970).
- ⁹R. Pinchaux, C. Chekroun, Y. Petroff, and M. Balkanski, Europhysics Conference on the Physics of Se and Te, Pont-à-Mousson, France, 1971 (unpublished); C. Chekroun, thesis (Paris, 1972) (unpublished).
- ¹⁰P. Nielsen, Phys. Rev. B **6**, 3739 (1972).
- ¹¹N. V. Smith and M. M. Traum, Phys. Rev. Lett. **25**, 1017 (1970).
- ¹²L. D. Laude, B. Fitton, and M. Anderegg, Phys. Rev. Lett. **26**, 637 (1971).
- ¹³L. D. Laude, B. Fitton, B. Kramer, and K. Maschke, Phys. Rev. Lett. **27**, 1053 (1971).
- ¹⁴K. Maschke, L. D. Laude, and B. Kramer (unpublished).
- ¹⁵C. Benoit-à-la-Guillaume and J. M. Debever, Solid State Commun. **3**, 19 (1965).
- ¹⁶C. Rigaux and M. Serrero, Solid State Commun. **3**, 21 (1965).
- ¹⁷G. G. Roberts, S. Tutihasi, and R. C. Keezer, Phys. Rev. **166**, 637 (1968); R. Fischer, Phys. Status Solidi **31**, K139 (1969).
- ¹⁸W. Henrion, Phys. Status Solidi **20**, K145 (1967).
- ¹⁹S. Tutihasi and I. Chen, Phys. Rev. **158**, 623 (1967).
- ²⁰S. Tutihasi, G. G. Roberts, R. C. Keezer, and R. E. Drews, Phys. Rev. **177**, 1143 (1969).
- ²¹J. Stuke and H. Keller, Phys. Status Solidi **7**, 189 (1964); Phys. Status Solidi **8**, 831 (1965).
- ²²E. Mohler, J. Stuke, and G. Zimmerer, Phys. Status Solidi **22**, K49 (1967).
- ²³A. G. Leiga, J. Opt. Soc. Am. **58**, 880 (1968).
- ²⁴R. Sandrock, Phys. Status Solidi B **43**, 199 (1971).
- ²⁵U. Gerhard, Adv. Solid State Phys. **10**, 175 (1970).
- ²⁶E. O. Kane, Phys. Rev. **175**, 1039 (1968).
- ²⁷The usual way of overcoming this difficulty is to cesiate the materials studied, which brings the threshold down to 1.8–2.0 eV. An attempt was made in that direction in the case of trigonal Te, but the cesiation yielded the formation of Cs₂Te with a photoelectric threshold of 3.5 ± 0.1 eV.
- ²⁸R. A. Pollak, S. Kowalczyk, L. Ley, and D. A. Shirley, Phys. Rev. Lett. **29**, 274 (1972).
- ²⁹G. Weiser and J. Stuke, in *Proceedings of the Ninth International Conference on the Physics of Semiconductors, Moscow, 1968* (Nauka, Leningrad, 1968).
- ³⁰R. C. Keezer, C. Wood, and J. W. Moody, J. Phys. Chem. Solids Suppl. **1**, 119 (1967).
- ³¹M. R. Barnes and L. D. Laude, Rev. Sci. Instrum. **42**, 1191 (1971).
- ³²P. Lukirsky, Z. Phys. **22**, 351 (1924).
- ³³R. C. Eden, Rev. Sci. Instrum. **41**, 252 (1970).
- ³⁴The EDC total width is practically independent of slit-opening changes in the range 0.1–1 mm. These variations introduce energy-error fluctuations of the order of 30-meV maximum in that range, at $h\nu = 7.72$ eV.
- ³⁵H. B. Holl, J. Opt. Soc. Am. **57**, 683 (1967).
- ³⁶J. M. Ballantyne, Phys. Rev. B **6**, 1436 (1972).
- ³⁷C. G. Ribbing, D. T. Pierce, and W. E. Spicer, Phys. Rev. B **4**, 4417 (1971); D. T. Pierce and W. E. Spicer, Phys. Rev. B **5**, 3017 (1972).
- ³⁸W. E. Rudge, C. D. Chekroun, and I. B. Ortenburger, Bull. Am. Phys. Soc. **18**, 350 (1973); and unpublished.
- ³⁹J. Stuke and G. Zimmerer (unpublished).
- ⁴⁰R. C. Eden, Ph.D. thesis (Stanford University, 1967) (unpublished).
- ⁴¹L. D. Laude, R. F. Willis, and B. Fitton, Phys. Rev. Lett. **29**, 472 (1972).
- ⁴²N. F. Mott, Adv. Solid State Phys. **9**, 22 (1969); Philos. Mag. **19**, 835 (1969).
- ⁴³Electron-surface scattering introduced by surface contamination is associated with a shift of E_T to lower energy in trigonal Te. Such a shift is not observed here, where the low-energy onset of the EDC's remains at the same position, independent of photon energy. Surface scattering associated with surface dislocations can reasonably be assumed to be negligible in view of the high-quality cleavages performed on the Te crystals used in this work (for a discussion of this problem, see, for instance, Ref. 55).
- ⁴⁴L. D. Laude and B. Fitton, J. Non-Cryst. Solids **8–10**, 971 (1972).
- ⁴⁵A. V. Sandulova, I. D. Gortynskaya, A. E. Nosenko, and A. D. Gonsharov, Fiz. Tekh. Poluprovodn. **6**, 976 (1962) [Sov. Phys.-Semicond. **6**, 850 (1972)].
- ⁴⁶M. J. Capers and M. White, Thin Solid Films **8**, 353 (1971).
- ⁴⁷M. Paesler, Bull. Am. Phys. Soc. **18**, 472 (1973).
- ⁴⁸C. N. Berglund and W. E. Spicer, Phys. Rev. **136**, A1030 (1964). In Eq. (7), all excited electrons are implicitly assumed to propagate in the bulk, i.e., they all have the same drift mobility. This implies necessarily that localized states are not involved in the optical excitation process. This condition is fulfilled for transitions occurring between delocalized (or extended) states (Ref. 42) lying, say, a few tenths of an eV below the p_2 valence band edge and above the bottom of the second conduction band in disordered Te. For transitions involving localized states, about the band edges or in the band gaps, hopping or tunneling

- mechanisms take place which affect the drift mobility of the actual electrons. Such transitions contribute to spectral features appearing at the edges of the EDC's. It seems clear that these features cannot be described by Eq. (7), but rather by an expression of the photocurrent containing explicitly a transport parameter (the drift mobility, for example) as shown in Ref. 41.
- ⁴⁹W. M. Hartmann and S. D. Mahanti, *J. Non-Cryst. Solids* **8-10**, 633 (1972).
- ⁵⁰D. C. Koningsberger, J. H. M. C. v. Wolput, and P. C. V. Rieter, *Chem. Phys. Lett.* **8**, 145 (1971); D. Brown, D. S. Moore, and E. F. W. Seymour, *J. Non-Cryst. Solids* **8-10**, 256 (1972).
- ⁵¹J. R. Dixon and J. M. Ellis, *Phys. Rev.* **123**, 1560 (1961); see also A. H. Sommer, *Photoemissive Materials* (Wiley, New York, 1968), p. 10.
- ⁵²J. Stuke, *Phys. Status Solidi* **6**, 441 (1964).
- ⁵³T. H. Keil, *Phys. Rev.* **144**, 582 (1966).
- ⁵⁴H. J. Queisser, in *The Physics of Sc and Tc*, edited by W. C. Cooper (Pergamon, Oxford, England, 1969), p. 289.
- ⁵⁵G. W. Gobeli and F. G. Allen, *Phys. Rev.* **127**, 141 (1962).
- ⁵⁶R. Pinchaux (private communication).
- ⁵⁷G. Lucovsky, A. Mooradian, W. Taylor, G. B. Wright, and R. C. Keezer, *Solid State Commun.* **5**, 113 (1967).
- ⁵⁸P. Nielsen, *Solid State Commun.* **9**, 1745 (1971).
- ⁵⁹L. D. Laude (unpublished).
- ⁶⁰A. Axmann, W. Gissler, and T. Springer, in Ref. 54, p. 299.
- ⁶¹G. Lucovsky, in Ref. 54, p. 255; and *Mater. Res. Bull.* **4**, 505 (1969); R. Kaplow, T. A. Rowe, and B. L. Averbach, *Phys. Rev.* **168**, 1068 (1968).
- ⁶²M. H. Brodsky, R. J. Gambino, J. E. Smith, Jr., and Y. Yacoby, *Phys. Status Solidi B* **52**, 609 (1972); A. Koma and S. Tanaka, *J. Non-Cryst. Solids* **8-10**, 251 (1972).
- ⁶³H. Richter and G. Breitling, *Z. Naturforsch. A* **26**, 1699 (1971).
- ⁶⁴H. Richter, *J. Non-Cryst. Solids* **8-10**, 388 (1972); see also N. B. Zakharova and Yu. A. Cherkasov, *Fiz. Tverd. Tela* **12**, 1977 (1970) [*Sov. Phys.-Solid State* **12**, 1572 (1971)].
- ⁶⁵R. C. Keezer (private communication).
- ⁶⁶T. Ichikawa, *Phys. Status Solidi* **56**, 707 (1973).
- ⁶⁷G. Tourand and M. Breuil, *J. Phys. (Paris)* **32**, 813 (1971); G. Tourand, B. Cabane, and M. Breuil, *J. Non-Cryst. Solids* **8-10**, 676 (1972).
- ⁶⁸B. Cabane and J. Friedel, *J. Phys. (Paris)* **32**, 73 (1971).